

1 **SHORT TITLE:** Effects of loss of ALB3b insertase in diatoms

2

3 **CORRESPONDING AUTHOR:** Marianne Nymark ([marianne.nymark@ntnu.no](mailto:marianne.nymark@ntnu.no))

4

5 **Loss of ALBINO3b insertase results in a truncated light-harvesting antenna in diatoms**

6 Marianne Nymark\*<sup>#1</sup>, Charlotte Volpe\*<sup>2</sup>, Marthe Caroline Grønbech Hafskjold<sup>1</sup>, Henning  
7 Kirst<sup>3</sup>, Manuel Serif<sup>1</sup>, Olav Vadstein<sup>2</sup>, Atle Magnar Bones<sup>1</sup>, Anastasios Melis<sup>3</sup>, Per Winge<sup>1</sup>.

8 \*Joint first author

9 <sup>1</sup>Department of Biology, Norwegian University of Science and Technology, N-7491, Trondheim,  
10 Norway

11 <sup>2</sup>Department of Biotechnology and Food Science, Norwegian University of Science and  
12 Technology, N-7491, Trondheim, Norway

13 <sup>3</sup>Department of Plant and Microbial Biology, UC Berkeley, Berkeley, California 94720, USA

14

15 **ONE SENTENCE SUMMARY:**

16 Diatom ALB3b is required for insertion of Fx-Chl binding proteins in thylakoid membranes, and  
17 has a novel conserved domain implying different interaction partners from those in plants/green  
18 algae.

19

20 **AUTHOR CONTRIBUTIONS:**

21 M.N., A.M.B., O.V., A.M. and P.W. conceived the research plans. M.N., A.M.B., A.M. and  
22 P.W. supervised and designed the experiments. M.N., C.V., M.C.G.H., H.K and M.S. performed  
23 the experiments. M.N., C.V., M.C.G.H., H.K, A.M. and P.W. analyzed the data. M.N. and C.V.  
24 wrote the article with contributions of all the authors. M.N. agrees to serve as the author  
25 responsible for contact and ensures communication.

26

27

28 **FUNDING:**

29 This work was supported by a grant from the Research Council of Norway to A.M.B through  
30 funding of the project “Downsizing light harvesting antennae to scale up production potential  
31 and valorization from cultivation of marine microalgae” (project no. 267474), a Peder Sather  
32 Grant Award to A.M. and A.M.B. (Peder Sather Foundation Grant Number: SRPSC4 1-50504-  
33 13618-44 ME1AM), the NTNU enabling technologies program to P.W., and a grant from the  
34 Research Council of Norway to O.V. through funding of the project Microbially Produced Raw  
35 Materials for Aquafeed (MIRA; project no. 239001).

36

37 **AUTHOR FOR CONTACT:** [marianne.nymark@ntnu.no](mailto:marianne.nymark@ntnu.no) (Marianne Nymark)

38

39 **ABSTRACT**

40 The family of chloroplast ALBINO3 proteins function in the insertion and assembly of thylakoid  
41 membrane protein complexes. Loss of ALB3b in the marine diatom *Phaeodactylum tricorutum*  
42 leads to a striking change of cell color from the normal brown to green. A 75% decrease of the  
43 main fucoxanthin-chlorophyll *a/c*-binding proteins was identified in the *alb3b* strains as the  
44 cause of changes in the spectral properties of the mutant cells. The *alb3b* lines exhibit a truncated  
45 light-harvesting antenna phenotype with reduced amounts of light harvesting pigments and  
46 require a higher light intensity for saturation of photosynthesis. Accumulation of photoprotective  
47 pigments and LHCX proteins were not negatively affected in the mutant strains, but still the  
48 capacity for non-photochemical quenching was lower compared to wild type. In plants and green  
49 algae, ALB3 proteins interact with members of the chloroplast signal recognition particle  
50 pathway through a lysine-rich C-terminal domain. A novel conserved C-terminal domain was  
51 identified in diatoms and other stramenopiles, questioning if ALB3b proteins have the same  
52 interaction partners as its plant/green algae homologs.

53

54 **INTRODUCTION**

55 Diatoms (*Bacillariophyceae*) are a major group of eukaryotic phytoplankton belonging to the

56 phylum Heterokont that evolved through a secondary endosymbiotic event around 200 to 180  
57 million years ago (Brown and Sorhannus, 2010). Diatoms are key primary producers in the  
58 marine food chain. They account for 40% of the total carbon fixation in oceans and 25% of the  
59 total global oxygen production (Falkowski et al., 1998). Diatom plastids differ significantly from  
60 the ones in green algae and higher plants due to their peculiar inheritance and evolution (Oudot-  
61 Le Secq et al., 2007). Because of secondary endosymbiotic events, four membranes surround the  
62 diatom chloroplast. The outer envelope, known as chloroplast endoplasmic reticulum, is a  
63 continuum with the nuclear envelope. The diatom thylakoids are organized in stacked bands of  
64 three membranes, also known as girdle lamellae, spanning along the entire length of the plastid.  
65 This configuration differs significantly from the classic grana stacks and interconnecting stroma-  
66 exposed thylakoids organization found in higher plant chloroplasts (Austin and Staehelin, 2011).  
67 Light harvesting complexes (LHCs) are embedded in the thylakoid membrane of the chloroplast  
68 and surround the photosynthetic reaction centers of the photosystems.

69 In contrast to higher plants, where specific LHCs serve either PSI or PSII, diatoms are  
70 characterized by a peripheral fucoxanthin (Fx)-chlorophyll (Chl) *a/c* antenna complex believed  
71 to deliver excitation energy to both photosystems, in addition to having a PSI associated antenna  
72 (Lepetit et al., 2010; Büchel, 2015). Proteins of the peripheral Fx-Chl *a/c* antenna complex in  
73 diatoms belong to the LHC superfamily (Durnford et al., 1996), but are often referred to as Fx-  
74 Chl *a/c* binding proteins (FCPs) in order to distinguish them from the LHCs of the green lineages  
75 (Falkowski and Raven, 2007). In addition to the light harvesting pigments, FCPs also bind  
76 diadinoxanthin (Ddx) and diatoxanthin (Dtx), photoprotective pigments essential during light  
77 stress conditions (Wang et al., 2019). The FCPs belong to three major LHC classes: the LHCF,  
78 including the main Fx-Chl *a/c* binding proteins, the red algal-like LHCRs, and the LHCXs,  
79 related to the LhcSRs in *Chlamydomonas reinhardtii* (Büchel, 2015). The latter has been shown  
80 to play a central role in dissipating excessively absorbed energy through non-photochemical  
81 quenching (NPQ) in cooperation with photoprotective pigments (Bailleul et al., 2010; Taddei et  
82 al., 2016; Lepetit et al., 2017; Taddei et al., 2018).

83

84 LHC proteins and certain photosystem core proteins are known to be integrated into the  
85 thylakoid membrane of higher plants and green microalgae through the post-translational or co-

86 translational part of the chloroplast signal recognition particle (CpSRP) assembly pathway  
87 (Sundberg et al., 1997; Schuenemann et al., 1998; Bellafiore et al., 2002; Gerdes et al., 2006;  
88 Kirst et al., 2012; Kirst et al., 2012; Kirst and Melis, 2014). The plant/green algae CpSRP  
89 pathway includes the LHC specific chaperon CpSRP43, the GTPase CpSRP54, the signal  
90 recognition receptor CpFTSY and the ALBINO3 insertase (ALB3) (Bellafiore et al., 2002; Kirst  
91 and Melis, 2014). Homologues of CpSRP54, CpFTSY and ALB3 can be identified in diatom  
92 genomes (Armbrust et al., 2004; Bowler et al., 2008; Mock et al., 2017), whereas no homologue  
93 for the molecular chaperon CpSRP43 have been identified (Träger et al., 2012). CpSRP43  
94 orthologues appear to be restricted to plants and green algae, however distantly related ankyrin  
95 repeat proteins can be found in Haptophyceae. Diatom CpSRP54 knockout mutants have been  
96 shown to be light sensitive (Nymark et al., 2016), but no further information exists about  
97 CpSRP54's role, or the role of any other members of the CpSRP pathway, in integration and  
98 assembly of thylakoid membrane proteins in diatoms. It has been shown, however, that efficient  
99 integration of FCPs depend on stromal factors and on the presence of GTP (Lang and Kroth,  
100 2001).

101

102 In higher plants and green microalgae, members of the CpSRP pathway guide certain chloroplast  
103 proteins to the thylakoid membranes where ALB3 mediates protein insertion in the developing  
104 thylakoids. ALB3 belongs to the YidC/Oxa1/Alb3 family of proteins functioning in folding,  
105 insertion and assembly of membrane protein complexes in bacteria and in certain eukaryotic  
106 organelles, such as mitochondria and chloroplasts (Hennon et al., 2015). The homologs within  
107 each subfamily have different C-terminal domains that are crucial for their function and protein-  
108 protein interaction. Two homologs belonging to this protein family are found in the chloroplasts  
109 of *Arabidopsis thaliana*, ALB3 and ALB4 (Sundberg et al., 1997; Gerdes et al., 2006) and *C.*  
110 *reinhardtii*, ALB3.1 and ALB3.2 (Bellafiore et al., 2002). ALB3 mutants of *A. thaliana* have a  
111 severe phenotype. They are characterized by white/pale-yellow leaves, are defective in thylakoid  
112 membrane development, have strongly decreased pigment content and are unable to survive  
113 phototrophically beyond the seedling stage when grown on soil (Sundberg et al., 1997). The *A.*  
114 *thaliana* ALB3 insertase is essential for insertion of LHC proteins through the post-translational  
115 CpSRP pathway and seems to be involved in co-translational assembly of certain chloroplast  
116 encoded membrane proteins (Sundberg et al., 1997; Moore et al., 2000; Kugelman et al., 2013).

117 Functional data exist also for the two *C. reinhardtii* ALB3 homologs, ALB3.1 and ALB3.2  
118 (Bellafiore et al., 2002; Ossenbühl et al., 2004; Göhre et al., 2006). The ALB3.1 of *C. reinhardtii*  
119 has been shown to be crucial for insertion of LHC proteins into the developing thylakoid  
120 membrane and to play a role in the assembly of D1 reaction center protein into PSII (Bellafiore  
121 et al., 2002; Ossenbühl et al., 2004). In contrast to the *A. thaliana* ALB3 mutants, *C. reinhardtii*  
122 cells lacking ALB3.1 are still capable of phototrophic growth. The other *C. reinhardtii* ALB3  
123 homolog, ALB3.2, is however essential for cell survival and is believed to be associated with the  
124 assembly and maintenance of the photosystems (Göhre et al., 2006).

125

126 Important differences have been identified between the function of the ALB3 homologs of  
127 organisms within the green lineage. We therefore hypothesized that characterization of diatom  
128 ALB3 insertases have the potential to uncover new and unique functional features connected to  
129 this protein family. Using a reverse genetics approach, we applied the CRISPR/Cas9 technology  
130 to knock out *ALB3b*, encoding one of the two ALB3 proteins present in the diatom  
131 *Phaeodactylum tricornutum*. We demonstrate here that ALB3b's primary functional role pertains  
132 to insertion of light-harvesting antenna proteins in the developing thylakoid membrane. This,  
133 however, does not include antenna proteins functioning in photoprotection. Reduced levels of  
134 light-harvesting antenna proteins resulted in changes in the spectral properties, pigment content,  
135 growth rate and photosynthetic performance of the cells.

136

## 137 **RESULTS**

138 Two homologs of the ALB3 insertase were identified in *P. tricornutum* and in all other  
139 stramenopiles where sequence data are available (Supplementary Figure S1). Phylogenetic  
140 analyses showed that ALB3 proteins in plants/green algae and ALB3 proteins from  
141 stramenopiles were clearly divided into two distinct groups (Supplementary Figure S1).  
142 Sequence similarity with the two ALB3 proteins with known functions in the green algae *C.*  
143 *reinhardtii* could therefore not be used to predict the individual function of the two *P.*  
144 *tricornutum* ALB3 proteins (ALB3a and ALB3b). The ALB3a paralog has a basic lysine-rich C-  
145 terminal domain (CTD) with similarities to CTD domains in ALB3 proteins in plants and green

146 algae (Supplementary Figure S2). In *A. thaliana* this domain has been reported to interact  
147 directly with CpSRP43 and CpSRP54·CpFTSY complexes (Falk et al., 2010; Falk and Sinning,  
148 2010; Lewis et al., 2010; Dünschede et al., 2011; Chandrasekar and Shan, 2017). ALB3b  
149 proteins in stramenopiles, however, do not contain the lysine-rich CTD but have instead a unique  
150 conserved domain (Figure 1). Both *P. tricornutum* *ALB3* genes (*ALB3a* (Phatr2\_43657) and  
151 *ALB3b* (Phatr2\_46411)) were targeted for CRISPR/Cas9-mediated disruption, but we were only  
152 able to generate viable KO-lines for the *ALB3b* gene. Three independent *alb3b* knockout lines  
153 (*alb3b-14*, *alb3b-16*, *alb3b-19*) with large insertions of different sizes toward the 5' end of the  
154 gene (Supplementary Figure S3) were identified and cultured from single cells. All insertions  
155 consisted of fragments of the vectors used for transformation and caused premature stop codons  
156 at the N-terminal part of the protein (Figure 1B). To verify that both alleles were mutated and  
157 that no WT sequence was present, allele-specific PCR was performed. Both alleles could be  
158 amplified in the WT whereas only one allele could be amplified in the mutant strains, indicating  
159 larger insertion or deletion events which prevent amplification of the other mutated allele by  
160 PCR (Supplementary Figure S4). Complementation of all three *alb3b* KO mutants with a codon  
161 modified *ALB3b* (to avoid gene editing) was performed to confirm that the phenotype described  
162 below was the result of a lack of a functional ALB3B insertase.

163

#### 164 **Spectral properties of WT and *alb3b* mutants**

165 Previous studies on green algae and plants showed that mutations causing a reduction in the size  
166 of the light harvesting antennae result in a pale green color of the chloroplasts (Sundberg et al.,  
167 1997; Bellafiore et al., 2002; Polle et al., 2003; Kirst et al., 2012; Kirst et al.; Oey et al., 2013;  
168 Gu et al., 2017). The diatom FCP complexes contain, in addition to Chl *a* and *c*, high amounts of  
169 Fx responsible for the golden-brown coloration of the diatom cells (Gundermann and Büchel,  
170 2014; Büchel, 2015; Wang et al., 2019). The absorption properties of Fx are strongly dependent  
171 on the protein environment, and undergo extreme bathochromic shifts upon protein binding,  
172 dividing the different Fx molecules into more red, green and blue absorbing complexes  
173 (Premvardhan et al., 2009; Premvardhan et al., 2010; Gundermann and Büchel, 2014; Wang et  
174 al., 2019). We therefore hypothesized that a distortion of the normal antenna size/structure of *P.*  
175 *tricornutum* could result in a visible change in cell coloration. Disruption of the gene encoding

176 the ALB3B insertase did indeed cause a change in coloration from the normal golden brown of  
177 the WT cells, to a green coloration, suggesting structural changes of the light harvesting antenna  
178 in the *alb3b* KO mutants (Figure 2A).

179

180 To further explore the visual changes in spectral properties in the *alb3b* mutants compared to  
181 WT cultures, we recorded the *in vivo* absorbance (Figure 2B) and fluorescence excitation spectra  
182 (Figure 2C) for medium light (ML) acclimated cultures. The spectra showed that less light  
183 energy in the blue-green region is absorbed and available for photosynthesis in cultures lacking  
184 the ALB3b insertase. *In vivo* fluorescence excitation spectra were used to indicate the pigments'  
185 relative energy transfer efficiency (ETE) to Chl *a* in the reaction center of PSII (RCII). The  
186 differences in the *in vivo* fluorescence excitation spectra between WT and *alb3b* mutants (Figure  
187 2C, inset) strongly resembled the absorption characteristics of Chl *c* (peak at 462 nm) and Fx (peak  
188 at 520 nm) (Bricaud et al., 2004; Premvardhan et al., 2009; Gundermann and Büchel, 2014),  
189 implying a significantly lower contribution in energy transfer from Chl *c* and Fx to RCII in the *alb3b*  
190 KO mutants. Smaller differences between WT and mutant strains are expected for the absorption  
191 spectra, as these spectra will also include pigments associated with PSI and non-protein bound  
192 carotenoids dissolved in the thylakoid membrane that do not transfer absorbed energy to PSII  
193 (Lepetit et al., 2010). Even so, the difference in the peak profile for the absorption spectra (Figure  
194 2B, inset) matches the difference in the *in vivo* fluorescence excitation spectra confirming a  
195 reduction of Chl *c* and Fx in the mutants.

196

197 Low temperature (77 K) fluorescence measurements were performed to clarify the distribution of  
198 excitation energy between PSII and PSI in WT compared to *alb3b* mutant cultures (Figure 3). The  
199 same samples were excited with either 435 nm (targeting Chl *a* absorption maxima; Figure 3A) or  
200 470 nm (targeting antenna pigments (Chl *c* and carotenoids; Figure 3B)). 77 K emission spectra  
201 recorded from ML acclimated samples revealed fluorescence emission maxima at 688 nm and 710  
202 nm, which are traditionally attributed to PSII and PSI, respectively (Ikeda et al., 2008; Yamagishi et  
203 al., 2010; Juhas and Buchel, 2012). In addition, an increase in fluorescence at 710 nm ( $F_{710}$ )  
204 emission at the expense of  $F_{687}$  was observed in *P. tricornutum* cells that were in a state of high NPQ  
205 (Lavaud and Lepetit, 2013). In WT samples the chosen excitation wavelengths caused a preferential  
206 energy transfer to PSII, displaying a relative amplitude of PSII fluorescence emission that was 2.5-

207 fold (435 nm) or 3.3-fold (470 nm) higher than the PSI emission ( $F_{687}/F_{710}$ ). In contrast, the average  
208  $F_{687}/F_{710}$  observed in the *alb3b* mutants were  $F_{687}/F_{710}= 1.3$  (435 nm) or 1.4 (470 nm), implying that  
209 excitation energy transfer to PSII was relatively more affected than energy transfer to PSI.

210

### 211 **Effect of lack of ALB3b insertase on the organization of photochemical apparatus**

212 The green color of the *alb3b* KO mutants and the combined results from the absorbance,  
213 fluorescence excitation and emission spectra suggested that these mutants have an altered  
214 functional light-harvesting antenna size. To investigate this in more detail the WT and the *alb3b*  
215 KO lines were analyzed using an absorbance difference spectrophotometer (Melis, 1989). The  
216 rate of light absorption per second by PSII and PSI was measured by using low intensity actinic  
217 light selected by cut-off and interference filters to selectively excite Fx (533 nm) or Chl *a* (670  
218 nm), respectively (Table 1). When exciting Fx, the rate of light utilization by the photosystems  
219 revealed a severe decrease in the absorption cross section both for PSII and for PSI in the *alb3b*  
220 mutant lines compared to WT (Table 1). The functional Chl *a* antenna size of PSII and PSI in  
221 the mutants were less affected because of the Chl *a* molecules bound to the photosystem core  
222 subunits (Ben-Shem et al., 2003; Nelson and Yocum, 2006; Ago et al., 2016) (Table 1). In  
223 accordance with the 77 K data, these data also suggest a more severe decrease of the antenna  
224 size of the PSII compared to the PSI (Table 1).

225

226 Organization of the photochemical apparatus was further studied by quantification of PSI (P700)  
227 relative to the Chl *a* content of the cells. P700 content was measured from the light induced  
228  $\Delta A_{700}$  absorbance change at 700 nm attributed to photooxidation of P700. On a P700 basis, there  
229 was a substantially lower number of Chl *a* molecules in the *alb3b*, i.e., from 663 Chl *a*/P700 in  
230 the WT, down to an average of 425 Chl *a*/P700 in the mutants (Table 1). This directly reflects  
231 the lowering of Chl *a* pigments per electron-transport chain (i.e., per P700) in the *alb3b* mutants  
232 relative to the WT.

233

234 Western blot was used for examination of the role of the ALB3b insertase in incorporating  
235 proteins in the thylakoid membrane. Antibodies specific for antenna proteins (LHCFs and  
236 LHCXs) and photosystem subunits (D1, D2 and PsaC) were used, and an antibody against AtpB  
237 was employed as loading control. The level of LHCF proteins in the *alb3b* mutants was assessed



238 by an antibody binding to a highly conserved epitope of the LHCF1 to LHCF11 proteins (Juhas  
239 et al., 2014), and found to be lowered to about 25% of WT levels in cells grown under both LL  
240 and ML conditions (Figure 4A). The relative decline of LHCF proteins is in good agreement  
241 with the smaller functional antenna size of PSII, as estimated from the kinetic  
242 spectrophotometric measurements using Fx excitation (Table 1). The relative gene expression  
243 levels of four *LHCF* genes (*LHCF1*, *LHCF2*, *LHCF5* and *LHCF8*) were examined to determine  
244 if the low content of LHCF proteins in the *alb3b* lines could be explained by a strong  
245 downregulation of the expression of these genes. Our data showed high gene expression levels  
246 (low Ct-values) of the examined *LHCFs* in all lines (Supplementary Table S1). Of the examined  
247 LHCF genes, only *LHCF8* was significantly, but moderately, down-regulated in all *alb3b* lines  
248 (Supplementary Figure S5). No antibodies are available for detection of LHCR proteins  
249 constituting the main LHC protein fraction associated the PSI antenna (Lepetit et al., 2010;  
250 Grouneva et al., 2011; Gundermann and Büchel, 2014). However, the smaller functional PSI  
251 antenna size in the mutant lines implied that ALB3b plays a vital role also in insertion of LHCR  
252 proteins. An antibody (anti-FCP6) against an LHCX (FCP6) of *Cyclotella meneghiniana*, which  
253 also cross-react with the *P. tricornutum* LHCX proteins (Juhas et al., 2014), was used for  
254 comparison of the relative content of these photoprotective proteins. LHCX1 is crucial for NPQ  
255 to take place, whereas LHCX2-3 can provide additional NPQ capacity during high light stress  
256 (Bailleul et al., 2010; Lepetit et al., 2017; Taddei et al., 2016; Taddei et al., 2018). LHCX1 and  
257 LHCX3 are of highly similar size (21.9 kDa and 22.8 kDa, respectively), therefore complete  
258 separation by western blot analysis is challenging. Based on the expression pattern of the LHCX  
259 isoforms known from literature, we interpret the proteins detected under both LL and ML  
260 conditions to be a mix of LHCX1 and LHCX3 with the major contribution coming from LHCX1  
261 under these conditions (Taddei et al., 2016; Taddei et al., 2018). The relative content of the  
262 LHCX1+3 proteins in the mutants compared to WT seemed to be unaffected (slightly reduced  
263 levels of LHCX1+3 in *alb3b-14*) in both light conditions (Figure 4A). The LHCX2 protein (24.7  
264 kDa) was detected at similar levels in WT and *alb3b* lines after 6 h of ML exposure  
265 (Supplementary Figure S8B), but it was not detectable in LL or ML-acclimated samples (Figure  
266 4A). The strong band of ~22 kDa detected in WT and *alb3b* lines 6 h after the shift from LL to  
267 ML (Supplementary Figure S8B) is likely to contain large amounts of LHCX3 in addition to  
268 LHCX1 (Taddei et al., 2016; Taddei et al., 2018). Based on Western blot analyses performed on

269 PSI/II core proteins, the lack of a functional ALB3b insertase does not seem to have a negative  
270 impact on the incorporation of chloroplast-encoded photosystem subunits (Figure 4B).

271 Preliminary analysis with transmittance electron microscopy (TEM) showed a lower number of  
272 thylakoid membranes per chloroplast, but no obvious difference in the thylakoid architecture  
273 could be observed in the *alb3b-14* mutant line acclimated to LL (Supplementary Figure S6).

274

### 275 **Functional properties of the *alb3b* KO mutants**

276 To study the capability of the *alb3b* mutant to respond to a shift in light conditions, LL  
277 acclimated cells (0 h) were shifted to ML conditions and sampled after 0.5, 6, 24, 48 and 168 h.  
278 The pigment content (Figure 5) and photosynthetic performance (Figure 6 and Figure 7) of the  
279 acclimating cells were analyzed.

280

### 281 **Capacity for photoacclimation and photoprotection**

282 As expected from the changed coloration and spectroscopic analyses, the *alb3b* KO mutants had  
283 a significantly lower content of light-harvesting pigments (LHPs) per cell compared to WT  
284 (Figure 5). Even though the content of LHPs in LL-acclimated *alb3b* mutants was already lower  
285 than in ML-acclimated WT cells, the LHP concentration in the mutants decreased further as a  
286 response to the ML-treatment (Figure 5A-B). This observation implies that the mechanisms  
287 controlling the downregulation of the LHPs in response to an increase in available light are  
288 independent of the actual pigment concentration in the cells. The *alb3b* mutant lines contained  
289 ~40-60 % less Chl *a* and ~60-65 % less Fx in response to the light treatment (Figure 5A-B,  
290 Supplementary Table S2).

291 The smaller antennae size of the mutant lines had no negative impact on the cell content of the  
292 xanthophyll cycle carotenoids Ddx and Dtx (Figure 5C-D). Both WT and *alb3b* mutant lines  
293 showed the expected photoprotective response to a shift to a higher light intensity (Nymark et al.,  
294 2009), which could be observed as an immediate rise in Dtx concentration inversely to a  
295 decrease in Ddx concentration. The conversion of Ddx to Dtx peaked at the 0.5 h time point as  
296 evident by the de-epoxidation state (DES) index (Figure 6A). The DES index decreased and

297 stabilized at a lower level after prolonged exposure to ML, indicating that the algae were  
298 acclimating to the new light condition. Although changes in DES index for both WT and mutants  
299 followed the same pattern after the shift to higher light intensities, the DES index were higher in  
300 the mutants than in WT cultures at all time points. The NPQ capacity of the *alb3b* mutants was  
301 initially (approx. two months after isolation of mutated single cells) found to be lowered to  
302 around half of that in the WT levels at irradiance levels  $> 400 \mu\text{mol m}^{-2} \text{s}^{-1}$  (Figure 6B), but when  
303 the same experiment was repeated after the cells had been maintained in culture for one more  
304 year (approx. 100-150 generations) the differences between WT and mutants had declined for all  
305 lines (Figure 6C). Measurements of time-dependent NPQ development in *alb3b* mutants and WT  
306 produced highly similar results as when calculating NPQ from rapid light curves (Supplementary  
307 Figure S7). The NPQ of *alb3b-16* was closer to WT-levels whereas a lower NPQ was observed  
308 in the two other *alb3b* lines. The smaller differences in NPQ capacity between *alb3b* lines and  
309 WT led us to also re-analyze the relative LHCF protein content, pigment levels and  
310 photosynthetic parameters in LL-acclimated *alb3b* and WT cultures after one more year of  
311 growth (Supplementary Figure S8A, Supplementary Figure S9 and Supplementary Figure S10).  
312 No major changes were observed for the *alb3b* lines relative to WT cells compared to the initial  
313 analyses of these parameters.

314

### 315 **Photosynthetic performance**

316 Variable Chl *a* fluorescence (PAM) was used to calculate the photosynthetic (PSII) efficiency  
317 ( $F_v/F_m$ ) of WT and mutant lines during the light experiment. In LL acclimated cells, the  $F_v/F_m$   
318 were  $\sim 0.7$  for all lines (Figure 7A), which is around the maximum value expected for algal cells  
319 under optimal growth conditions (Falkowski and Raven, 2007). After 0.5 h of ML exposure, both  
320 WT and mutant cells showed a modest decrease in  $F_v/F_m$  (Figure 7A). The  $F_v/F_m$  in the mutant  
321 cultures stabilized close to  $\sim 0.6$  in ML, whereas  $F_v/F_m$  in WT cultures increased after prolonged  
322 exposure to ML. The maximum relative electron transport rate ( $rETR_{\text{max}}$ ) and light saturation  
323 index ( $E_k$ ) values increased as a function of ML exposure time in all cultures (Figure 7C-D), as  
324 the photoacclimation mechanisms enabled the cells to utilize the increased amount of light  
325 energy available for photosynthesis (Nymark et al., 2009). However, the *alb3b* mutants  
326 displayed, on average, a  $\sim 30$ - $40\%$  higher  $rETR_{\text{max}}$  and  $E_k$  compared to WT cultures, showing the

327 largest differences during the first part of the light experiment before the cells had been able to  
328 downsize the photosynthetic apparatus in response to the increased light intensities. Less  
329 pronounced differences in  $rETR_{max}$  and  $E_k$  were found between WT and *alb3b* cultures at the 24  
330 h time point due to a more rapid change in photoacclimation status in WT cells, probably  
331 because of a higher cell division rate as described below (Table 3). To further investigate the  
332 apparent increased photosynthetic performance of the *alb3b* KO lines indicated by the PAM  
333 measurement, light-saturation curves of photosynthesis (P-E curves) based on oxygen evolution,  
334 were measured for WT and *alb3b* KO lines acclimated to either LL (Figure 7E) or ML (Figure 7F).  
335 The maximum photosynthetic rate ( $P_{max}$  ( $\mu\text{mol O}_2/\text{mol Chl/s}$ ), the maximum light utilization  
336 coefficient ( $\alpha$ ) and the saturation intensity ( $E_s$ ) of photosynthesis ( $P_{max}/\alpha$  ( $\mu\text{mol photons m}^{-2} \text{s}^{-1}$ ))  
337 were calculated from the P-E curves (Table 2) (Powles and Critchley, 1980). When normalized to  
338 Chl *a*, the mutant lines showed a typical truncated light-harvesting antenna (TLA) - mutant  
339 phenotype with higher  $P_{max}$  and  $E_s$  and slightly lower  $\alpha$  compared to WT due to lower functional  
340 absorption cross-section caused by the smaller antenna (Kirst et al., 2014). Thus, it should be  
341 noted that these results do not indicate a higher photosynthetic performance per cell. In fact, when  
342 oxygen evolution was normalized per cell, the mutant lines showed a  $P_{max}$  similar to WT  
343 (Supplementary Figure S11). Also, the light saturation curves of the *alb3b* KO lines acclimated to  
344 LL showed a tendency of declining photosynthetic activity at light intensity  $> 1000 \mu\text{mol photons m}^{-2}$   
345  $\text{s}^{-1}$  (Figure 7E).

346

### 347 **Effect of light intensity on cell growth**

348 Growth parameters were calculated from the exponential phase in batch cultures of LL and ML  
349 acclimated cultures (Table 3; Supplementary Figure S12) to investigate how the changes in  
350 antennae size and composition affected the cell division rate. The results showed that WT cells  
351 grew faster than *alb3b* KO mutants at both light conditions, but a shift from LL- to ML-  
352 intensities diminished that growth rate gap between the *alb3b* KO mutants and WT (Table 3), as  
353 recently observed in other TLA mutants (Kirst et al., 2014; Formighieri and Melis, 2017). At ML  
354 conditions the WT cells already divided at a maximum rate slightly above two cell divisions per  
355 day (Fawley, 1984). We hypothesized that if the slower growth rate of the *alb3b* mutants were  
356 caused by a lower ability to capture light energy, increasing the light intensities should have a

357 positive effect on growth of the mutant cells. To investigate if a further increase in light intensity  
358 could close the growth rate gap, mutants and WT cells were acclimated to HL conditions (480  
359  $\mu\text{mol photons m}^{-2} \text{s}^{-1}$ ). The growth temperature was set to 23°C which supports the highest cell  
360 division rate in *P. tricornutum* (Fawley, 1984). During the HL acclimation period (two weeks),  
361 the majority of the cells in one of the *alb3b* lines (*alb3b-16*) changed from the fusiform  
362 morphotype to a rounded phenotype. The rounded cells showed a tendency for aggregation,  
363 making accurate counting necessary for growth rate calculations difficult. The attempt to  
364 acclimate *alb3b-16* to HL was repeated after the discovery of the strongly increased NPQ  
365 capacity in cells that had been maintained in culture for one year after isolation of single cells,  
366 but the HL treatment induced the same change in morphotype as previously observed. The two  
367 other *alb3b* lines did not show a change in morphotype during the HL acclimation period or  
368 during the following growth rate experiments, but prolonged HL treatment (months) including  
369 periods in stationary phase, induced the formation of the rounded cell type also in the two other  
370 *alb3b* lines. The same treatment did not provoke the formation of round cells in WT cultures.  
371 Growth curves are included in Supplementary Figure S13A. The growth rate calculations from  
372 the exponential part of the curve, showed that the WT cells still divided twice per day in HL,  
373 whereas the average maximal growth rate of the *alb3b* mutants dropped from 1.2 in ML to 0.8  
374 divisions per day under HL (Table 3). The physiological status of the cells, measured as  $F_v/F_m$ ,  
375 was monitored during the length of the growth experiment (Supplementary Figure S13B). The  
376 average  $F_v/F_m$  in WT cultures during the period of maximal growth, was found to be 0.63. In  
377 contrast, the corresponding  $F_v/F_m$  value in the *alb3b* mutants were 0.41, pointing to a higher  
378 degree of photodamage. In order to investigate presence of oxidative damage, levels of lipid  
379 peroxidation were measured for HL acclimated WT and mutant cells (*alb3b-14*, *alb3b-19*). The  
380 mutant lines did not show higher levels of lipid peroxidation compared to the WT  
381 (Supplementary Figure S14). Similar levels of xanthophyll pigments in the mutant compared to  
382 the WT could explain these results, considering their role in the stabilization and protection of  
383 the thylakoid membrane lipids from peroxidation (Hauvaux et al., 2007).

#### 384 **Complementation studies of *alb3b* mutants**

385 A plasmid containing the codon modified *ALB3b* under control of its native promoter was  
386 introduced to the three *alb3b* lines by biolistic bombardment. As a result, 70 of in total 75

387 transformed colonies regained their brown coloration. Six brown colonies (two colonies derived  
388 from each of the three complemented lines) were randomly picked and subjected to PCR analysis  
389 followed by sequencing. The introduction of the modified *ALB3b* gene and the absence of WT  
390 sequence were confirmed (Supplementary Figure S15). Three brown colonies (representing each  
391 of the three complemented mutant lines) were cultured for analyses of pigment and LHCF  
392 content. The results showed that the WT phenotype was recovered by introduction of the  
393 modified *ALB3b* gene (Figure 8).

394 **DISCUSSION**

395 **Effects of loss of the *P. tricornutum* ALB3b insertase**

396 The significantly lower level of antenna proteins belonging to the LHCF group (Figure 4A) indicate  
397 that the primary role of the *P. tricornutum* ALB3b insertase is the efficient integration of the main  
398 LHC proteins into the thylakoid membrane. However, a small functional antenna size is still  
399 assembled, implying a phenotype where some LHC proteins can be inserted through other thylakoid  
400 membrane insertion pathways, or that some functional redundancy exists between ALB3b and the  
401 uncharacterized diatom homolog ALB3a. The mainly unaffected levels of photoprotective LHCX  
402 proteins found in *alb3b* mutants (Figure 4A) clearly indicate presence of other integration  
403 pathway(s) for antenna proteins. The lower level of LHPs and smaller functional antenna size, the  
404 changed spectral properties and the increased light saturation level, can be seen as effects of the  
405 lower amount of antenna proteins causing a truncated light harvesting antenna. The phenotypic  
406 traits listed above are characteristic for TLA-phenotype mutants, previously generated in  
407 cyanobacteria, green microalgae and higher plants (Polle et al., 2003; Kirst et al., 2012; Kirst et al.,  
408 2012; Kirst et al., 2014; Formighieri and Melis, 2017; Gu et al., 2017; Kirst et al., 2017; Kirst et al.,  
409 2018). TLA mutants have been shown to grow at relatively similar rates as WT when enough light  
410 energy is available (Bellafiore et al., 2002; Polle et al., 2003; Kirst et al., 2014; Gu et al., 2017).

411

412 The slow growth of the *alb3b* mutants compared to WT cells might be partially explained by a  
413 reduced ability to capture light energy, since an increase in light intensity from 35 (LL) to 200  $\mu\text{mol}$   
414  $\text{photons m}^{-2} \text{s}^{-1}$  (ML) diminished the difference in growth rate between WT and mutant by a factor  
415 2. If the smaller antenna size of the mutants were the sole reason for the slow growth rate, a further  
416 increase in irradiance should further diminish the difference in growth between WT and mutant.  
417 Instead, analyses of algae cultures acclimated to HL ( $\sim 480 \mu\text{mol photons m}^{-2} \text{s}^{-1}$ ) revealed a  
418 negative effect on cell division rate, photodamage of the *alb3b* mutants and induction of a round  
419 cell phenotype. The round or oval cell shape has previously been reported to be associated with  
420 prolonged exposure to abiotic stress (De Martino et al., 2007; De Martino et al., 2011; Herbstova et  
421 al., 2017). The apparent increased photosynthetic capacity estimated for *alb3b* mutants at both LL  
422 and ML light conditions seems counter intuitive if the *alb3b* mutants are high light sensitive.  
423 However, these data are calculated from light-response curves where the algae are subjected to high

424 light intensities for relative short periods of time (minutes). The high light experienced by the algae  
425 during the generation of light-response curves might be too short for extensive photodamage to  
426 occur. However, mutants acclimated to LL conditions did show signs of photoinhibition observed  
427 as a decrease in oxygen production when exposed to light intensities  $> 1000 \mu\text{mol photons m}^{-2} \text{s}^{-1}$   
428 (Figure 7E).

429

430 NPQ is an important photoprotective mechanism providing the ability to dissipate excessively  
431 absorbed energy harmlessly as heat during high light exposure. In the *alb3b* mutants the NPQ  
432 capacity was reduced compared to WT levels (Figure 6B-C and Supplementary Figure S7),  
433 suggesting a reduced capability to handle prolonged high light exposure. Several studies show a  
434 convincing relationship between the amount of both LHCX and Dtx and the capacity for NPQ, and  
435 the presence of LHCX proteins and the conversion of protein bound Ddx to Dtx has been found to  
436 be essential for NPQ to take place (Lavaud et al., 2002; Bailleul et al., 2010; Lepetit et al., 2012;  
437 Lepetit et al., 2013; Lepetit et al., 2017; Taddei et al., 2018). The level of LHCX proteins and the  
438 content of the xanthophyll cycle pigments (Ddx+Dtx) were not negatively affected by the lack of  
439 ALB3b insertase. However, Ddx and Dtx are found in three different pools in diatoms, one located  
440 in a lipid shield around the FCPs, and two that are bound to antennae proteins connected to PSI or  
441 the peripheral FCP antenna, respectively (Lepetit et al., 2010). Only the protein bound fraction of  
442 the peripheral antennae contribute to NPQ after conversion of Ddx to Dtx (Lepetit et al., 2010).  
443 Because of the potential to store xanthophyll cycle pigments in the lipid phase of the thylakoid  
444 membrane, the amount of accumulated Ddx+Dtx that are protein bound might still be reduced even  
445 though the cell concentrations in the *alb3b* lines are similar or higher than in WT. The molecular  
446 role of LHCX and Dtx in NPQ is still elusive, and no data exists about the precise localization of  
447 FCPs or the LHCX proteins. The latest models for NPQ in diatoms suggest that there are two  
448 quenching sites (Q1 and Q2) present in the diatom thylakoids (Miloslavina et al., 2009; Büchel,  
449 2014; Lavaud and Goss, 2014; Goss and Lepetit, 2015; Giovagnetti and Ruban, 2017). NPQ at Q1  
450 is believed to involve physical detachment of FCP oligomers from PSII that in *P. tricornutum* can  
451 be measured as an increase in 77 K emission at 710 nm and as a decrease of PSII cross section  
452 (Lavaud and Lepetit, 2013; Giovagnetti and Ruban, 2017), whereas Q2 seems to take place in FCPs  
453 functionally connected to PSII, and involve antennae reorganization and aggregation of LHC  
454 trimers (Miloslavina et al., 2009; Büchel, 2014; Lavaud and Goss, 2014; Giovagnetti and Ruban,



455 2017). Q2 is suggested to be dependent on the presence of protein bound Dtx and provides a much  
456 higher level of NPQ compared to Q1 (Giovagnetti and Ruban, 2017). Despite the comparable  
457 content of photoprotective antenna proteins and pigments in WT and *alb3b* mutants, the strong  
458 decrease in *alb3b* antennae size might disturb crucial protein-pigment or protein-protein (e.g LHCF-  
459 LHCX) interactions potentially necessary for effective antenna aggregation (Q2) and lower the pool  
460 of detachable antenna involved in Q1. This might lead to the lower NPQ capacity observed in the  
461 *alb3b* mutants. However, the difference in NPQ capacity between *alb3b* lines and WT decreased  
462 after the *alb3b* lines had been maintained in culture for one additional year (approx. 100-150  
463 generations). The increase in NPQ compared to WT was especially prominent for *alb3b-16*. No  
464 major differences in pigment or LHCF content between the individual *alb3b* lines or changes in the  
465 pigment or LHCF ratios between *alb3b* and WT were observed that could explain the changes in  
466 NPQ capacity over time. The different NPQ levels in the mutants and the general increase in NPQ  
467 over time in the *alb3b* lines compared to WT levels can therefore not be explained by changes in  
468 antenna size over time. Giovagnetti and Ruban (Giovagnetti and Ruban, 2017) showed that the  
469 amount of antenna detached are not proportional to the level of NPQ, and that the NPQ can  
470 continue to increase without a further reduction of the PSII cross-section. We therefore suggest that  
471 the increase in NPQ over time is caused not by a larger pool of detachable antenna, but that the  
472 *alb3b* lines, over many generations, have been able to increase their capacity for NPQ at Q2 through  
473 an unknown mechanism.

474  
475 **Role of diatom ALB3b in integration of nucleus and plastid encoded proteins compared to**  
476 **ALB3 in green alge/plants**

477 The *P. tricornutum* ALB3b showed functional similarities with the *C. reinhardtii* homolog ALB3.1  
478 (Bellafiore et al., 2002; Ossenbühl et al., 2004). Both the diatom ALB3b and the green algae  
479 ALB3.1 play a role in insertion of LHC proteins into the thylakoid membrane (Bellafiore et al.,  
480 2002; Kirst and Melis, 2014), and loss of the insertase causes a notably smaller antenna size  
481 (Bellafiore et al., 2002). In addition, *C. reinhardtii* cells lacking ALB3.1 contain a significantly  
482 increased fraction of highly stable membrane inserted, but unassembled D1 protein (Ossenbühl et  
483 al., 2004). The D1 content in *C. reinhardtii alb3.1* mutants were half of that of WT cells. Based on  
484 the above described findings, an additional role in assembly of D1 into PSII was identified in green  
485 microalgae (Bellafiore et al., 2002; Ossenbühl et al., 2004). Subunits of PSI (PsaC), PSII (D1, D2)

486 and ATP synthase complex (AtpB) were not negatively affected by the absence of the ALB3b  
487 insertase in diatom cells (Figure 4B), but our analyses does not discriminate between unassembled  
488 proteins in the thylakoid membrane and proteins that are incorporated into photosynthetic  
489 complexes. More extensive protein analyses would be necessary to rule out a role of the diatom  
490 ALB3b insertase in integration/assembly of chloroplast encoded thylakoid membrane proteins.  
491 Assembled PSII complexes are fully functional in both *C. reinhardtii* (Ossenbühl et al., 2004) and  
492 *P. tricornutum alb3b* mutants (Figure 7A). We detected no differences in photosynthetic efficiency  
493 in LL acclimated cells between WT and mutants. This implies that even though the *alb3b* KO lines  
494 have a truncated antenna size, there is no difference in the probability of the trapped excitation  
495 energy to be used for photochemistry between WT and mutants. However, a less efficient repair of  
496 PSII from photodamage (Guenther and Melis, 1990) and an associated slower replacement of  
497 damaged D1, could explain the on average ~12-14% lower  $F_v/F_m$  measured in *alb3b* mutants during  
498 prolonged ML exposure, and the on average ~36% lower  $F_v/F_m$  observed in HL acclimated mutant  
499 cells. An efficient PSII repair mechanism including a more frequent replacement of photodamaged  
500 D1 is required during such conditions (Baroli and Melis, 1996; Theis and Schroda, 2016).  
501 Alternatively (or additionally), the PSII of the *alb3b* mutants might be more susceptible to  
502 photodamage because of the altered light harvesting antennae disturbing the normally efficient NPQ  
503 mechanism (Figure 6B-C) functioning in this algae (Lavaud and Goss, 2014). However, the  
504 transformation of the normally fusiform *alb3b-16* line into the rounded morphotype in HL  
505 regardless of having a lower (Figure 6B) or more similar (Figure 6C and Supplementary Figure S7)  
506 NPQ capacity as WT indicates that there are other reasons for why *alb3b* mutants are sensitive to  
507 HL.

508  
509 The *Arabidopsis thaliana alb3p* mutant has also been reported to be photosensitive. *Alb3p* require  
510 very low light intensities ( $12 \mu\text{mol photons m}^{-2} \text{s}^{-1}$ ) to produce detectable levels of photosynthetic  
511 complexes like LHC trimers and PSII monomers and dimers (Kugelmann et al., 2013). To explain  
512 the severe phenotype of the *Alb3p* mutants, additional functions beyond the CpSRP pathway have  
513 been suggested for ALB3p (Kugelmann et al., 2013). Based on phenotypic similarities between the  
514 *Alb3p* and mutants defective in carotenoid synthesis it has been speculated that the ALB3p has a  
515 role in integration and assembly of carotenoids into photosynthetic complexes (Kugelmann et al.,  
516 2013). The slow growth of the *P. tricornutum alb3b* mutants that cannot be compensated by  
517 increased light intensities, and the susceptibility to prolonged high light exposure, suggest

518 additional roles for the ALB3b insertase. A future comparison with other types of *P. triornutum*  
519 TLA mutants will be valuable for dissecting primary effects of the absence of ALB3b, from the  
520 secondary effects of having a truncated light harvesting antenna size.

521

## 522 **CONCLUSION**

523 Our results show that ALB3b is essential for assembly of a full-size light harvesting antenna in  
524 diatoms. In higher plants and green algae, ALB3 insertases are a part of the CpSRP pathway and the  
525 basic lysine-rich CTD is necessary for the interaction with other members of the pathway  
526 (Bellafiore et al., 2002; Chandrasekar and Shan, 2017). We also identified this domain within the  
527 ALB3a proteins of the stramenopiles, but not in the ALB3b proteins which has a unique CTD  
528 domain. The LHC specific chaperon CpSRP43 is one of the ALB3's known interaction partners  
529 through its lysine-rich CTD domain, but neither we nor others (Träger et al., 2012) could identify  
530 this chaperon in diatoms or other stramenopiles. Also, the *P. triornutum* CpSRP54 mutant was not  
531 reported to have a changed coloration, only to be light sensitive (Nymark et al., 2016). The different  
532 CTD domain in ALB3b proteins, the absence of CpSRP43 and the unchanged coloration of the  
533 diatom CpSRP54 mutant, imply that the ALB3b proteins have other interaction partners than  
534 ALB3a and ALB3 of plants/green algae. A hypothetical model for the role of diatom ALB3  
535 insertases is presented in Figure 9. For verification of the model, a more thorough investigation of  
536 the *P. triornutum* CpSRP54 mutant and characterization of diatom FTSY mutants should be  
537 performed. This will clarify if ALB3b is part of the post-translational CpSRP pathway, or if diatom  
538 LHC proteins are guided to ALB3b through other mechanisms.

539

## 540 **MATERIALS AND METHODS**

541 An axenic *P. triornutum* culture originating from the sequenced clone Pt1 8.6 (CCMP2561) was  
542 obtained from the culture collection of the Provasoli-Guillard National Center for Marine Algae and  
543 Microbiota (NCMA), Bigelow Laboratory for Ocean Sciences.

544

### 545 **Experimental conditions**

546 Axenic culturing of *P. triornutum* WT cells and the three *alb3b* KO lines (*alb3b-14*, *alb3b-16* and

547 *alb3b-19*) were performed as described previously unless otherwise stated (Nymark et al., 2009).  
548 Cell cultures were grown at 15°C under continuous cool white fluorescent light at scalar irradiance  
549 ( $E_{PAR}$ ) of  $\sim 35 \mu\text{mol photons m}^{-2} \text{s}^{-1}$  (LL), or  $\sim 200 \mu\text{mol photons m}^{-2} \text{s}^{-1}$  (ML). For the high light  
550 (HL) experiment the WT and the three independent *alb3b* KO lines were acclimated to 480  
551  $\mu\text{mol m}^{-2} \text{s}^{-1}$  and grown at 23°C in a Vötsch VB 1514 plant growth chamber (Vötsch  
552 Industrietechnik GmbH, Germany) equipped with metal halide lamps (Powerstar HQI-BT 400  
553 W/D). The cultures were kept in the exponential growth phase for at least three weeks under  
554 these conditions to ensure that all cells were fully acclimated prior to conducting measurements.

555  
556 For the spectrophotometric and kinetic analysis cells were grown in F/2 enriched artificial seawater  
557 media (Guillard and Ryther, 1962). To avoid carbon limitation during growth the media were  
558 supplemented with  $\text{NaHCO}_3$  (final concentration of 23.5 mM, pH=7.4). Cultures were grown at 25  
559 °C in 2 L glass bottles constantly stirred to ensure homogenous growth. Continuous illumination  
560 was provided by white fluorescent LED light tubes at ML. For the measurements 80-85% of the  
561 total culture volume was harvested during the mid-exponential growth phase.

562

### 563 **Growth rates**

564 Growth rates were estimated in batch cultures of WT and *alb3b* KO lines (three biological  
565 replicates) acclimated to LL, ML or HL using a starting concentration of 100.000 (ML, HL) or  
566 200.000 (LL) cells/ml. Counting was performed either manually using a Bürker-Türk counting  
567 chamber after fixation with Lugol's solution (LL samples) or with a BD Accuri C6 Flow  
568 Cytometer (BD Bioscience; ML and HL samples). For the latter, glutaraldehyde (2% final solution)  
569 was used for fixation of cells. Samples were excited by a 20 mW 488 nm Solid State Blue laser  
570 and chlorophyll fluorescence was measured by a  $>670 \text{ nm}$  optical filter (FL3). The average  
571 maximum growth rates (cell division/day) were calculated by using a mean of the growth rates  
572 from the three biological replicates during the exponential phase.

573

### 574 **Phylogenetic analyses**

575 ALBINO3 proteins in the NCBI (National Center for Biotechnology Information) protein database  
576 and from the iMicrobe transcriptome database (<https://www.imicrobe.us/>) were selected for  
577 phylogenetic analyses. Accession numbers for the protein sequences used in the analysis are listed

578 in Supplementary Table S4. The analysis involved 47 ALB3 proteins from plants and algae, each  
579 species was represented with two ALB3 paralogs (ALB3.1/ALB3.2 or ALB3a/ALB3b). The protein  
580 alignment was generated by using the ClustalX program (Thompson et al., 1997) and manually  
581 refined in GeneDoc 2.7.000 (Nicholas et al., 1997). The evolutionary relationships were estimated  
582 using Maximum Likelihood (ML) method based on the Le-Gascuel model (Le and Gascuel, 2008)  
583 and the Neighbor-Joining method (Saitou and Nei, 1987). The initial tree for both ML and NJ  
584 analyses was obtained automatically by applying Neighbor-Join and BioNJ algorithms to a matrix  
585 of pairwise distances, estimated using a JTT model and the trees with best topology were selected.  
586 For the ML-analyses a discrete Gamma distribution was used to model evolutionary rate differences  
587 among sites (using 5 categories). All positions with less than 80% site coverage were eliminated.  
588 Tree branch confidence values were calculated by running 1000 bootstrap replicates for NJ and 100  
589 replicates for ML. The phylogenetic analyses were conducted in MEGA7 (Kumar et al., 2016).

590

#### 591 **CRISPR/Cas9 gene editing of the ALB3b insertase**

592 All steps for performing CRISPR/Cas9 editing of the *ALB3b* insertase gene (Phatr2\_46411;  
593 XM\_002180751) including selection of target site, ligation of adapter for target of interest into the  
594 pKS diaCas9-sgRNA plasmid (Nymark et al., 2016), transformation of diatom cells, and screening  
595 and identification of cells with biallelic mutations, were performed as described in the published  
596 protocol for CRISPR/Cas9 gene editing in *P. tricornutum* (Nymark et al., 2017). *ALB3b* specific  
597 oligos for creation of the adapter inserted into the sgRNA cassette of the CRISPR/Cas9 vector, and  
598 primers used for screening of cells with CRISPR/Cas9-mediated mutations, are presented in  
599 Supplementary Table S5. Three *alb3b* KO lines named *alb3b-14*, *alb3b-16* and *alb3b-19* were  
600 selected for functional characterization. These three selected lines were checked for off-target  
601 mutations by PCR amplification and sequencing of the regions containing the five most likely off-  
602 target sites. To identify potential off-target sites, a custom-made Perl based script was used to  
603 search the genome for sites with high homology to seed (PAM-proximal) region of the target site.  
604 The script uses a string-based approach, which allows for up to 3 mismatches in the seed region.  
605 Off-targets are ranked after their similarity to the target site as well as the position of the  
606 mismatches. No off-target mutations were found at any of the investigated sites. The Phatr2 ID for  
607 the genes containing the potential off-target sites and primers used for the screening process are  
608 listed in Supplementary Table S5.

609

### 610 **Allele-specific PCR**

611 Allele-specific PCR was performed as an additional control as previously described (Serif et al.,  
612 2017). In short, primers for PCR were derived which include an allele-specific difference on the 3'  
613 terminal base (see primers in Supplementary Table S5), thereby preventing polymerases without  
614 proofreading function from amplifying the respective other allele. Both alleles were amplified  
615 separately using HiDi polymerase (myPols, Konstanz, Germany) according to the manufacturer's  
616 instructions.

617

### 618 **Isolation of thylakoid membranes**

619 Cells were harvested by centrifugation at 1000 g for 8 min at 4 °C. The pelleted cells were  
620 resuspended in 50 mM Tricine – NaOH (pH 7.8) in ice-cold isolation buffer containing 300 mM  
621 sucrose, 5 mM MgCl<sub>2</sub>, 10 mM NaCl, 2% PVP (w/v), 0.1% BSA (w/v) and 5 mM ascorbic acid. The  
622 pellet was washed twice with the described buffer to remove residual salts from the growth media.  
623 Cells were broken using a Branson 250 sonicator (pulse mode, 50% duty cycle, output power of 5)  
624 with a precooled tip for 45 s followed by 1 min of cooling in dim light. This process was repeated 4  
625 times to ensure rupture of the majority of the cells. Unbroken cells were removed by centrifugation  
626 at 6500 rpm for 10 min at 4 °C. The thylakoid suspension was centrifuged at 75,000 g for 45 min at  
627 4°C using a Beckman Coulter ultra-centrifuge. The thylakoid pellet was resuspended in 5 ml of ice-  
628 cold Tricine-NaOH (pH 7.8) buffer containing 10 mM NaCl and 5 mM Mg<sub>2</sub>Cl. Samples were  
629 measured immediately upon preparation.

630

### 631 **Spectrophotometric and kinetics analysis**

632 Photosystem kinetics and PSI quantitation analysis were performed using a laboratory-constructed  
633 absorbance difference spectrophotometer (Melis and Brown, 1980; Melis, 1989). The premise for  
634 this method is that, under light limiting conditions, the rate of primary photochemistry is directly  
635 proportional to the light-harvesting antenna size (Melis, 1989). PSI (P<sub>700</sub>) content was measured  
636 from the light-induced  $\Delta A_{700}$  using a differential extinction coefficient of 64 mM<sup>-1</sup> cm<sup>-1</sup> (Hiyama  
637 and Ke, 1972). Actinic excitation was provided in the red region of the spectrum using a  
638 transmittance interference 670 nm filter combined with a yellow cut-off filter (CS 3-69). The

639 reaction mixture contained 50-100  $\mu\text{M}$  Chl *a*, 0.02% SDS (w/v), 250  $\mu\text{M}$  methyl viologen (MV)  
640 and 2.5 mM Na-ascorbate. The sample was illuminated once prior to measuring to ensure oxidation  
641 of Cytochrome *c*<sub>6</sub> and possibly of Cytochrome *f*. 2-3 experimental replicates were measured, with  
642 at least three technical replicates taken. Chl *a* concentration in the samples was calculated after  
643 extraction in 90% acetone (v/v) for half an hour in the dark using the Jeffrey-Humphrey equation  
644 for diatoms (Jeffrey and Humphrey, 1975). Photocatalytic kinetics of the two photosystems were  
645 measured based on Chl *a* fluorescence induction for PSII and P<sub>700</sub> oxidation for PSI (Melis, 1989).  
646 Actinic illumination was provided in the red and green regions of the spectrum using narrow  
647 interference filters with transmittance peaks at 670 nm and a 533 nm. These filters were chosen  
648 after examination of the thylakoid absorbance spectra so that the 670 nm filter would excite  
649 predominantly Chl *a*, whereas the 533 nm filter would excite Fx and other carotenoids. Incident  
650 light intensity provided was 12  $\mu\text{mol photons m}^{-2} \text{s}^{-1}$  in the green and 2.1  $\mu\text{mol m}^{-2} \text{s}^{-1}$  in the red  
651 region. The reaction mixture for the fluorescence kinetic measurements contained approximately 5-  
652 10  $\mu\text{M}$  Chl *a* and 20  $\mu\text{M}$  3-(3,4-dichlorophenyl)-1,1-dimethylurea (DCMU), and that for the P700  
653 oxidation kinetics contained 100-200  $\mu\text{M}$  Chl *a*, 250  $\mu\text{M}$  MV and 20  $\mu\text{M}$  DCMU.

654

### 655 **Absorbance spectra**

656 To avoid light scattering, absorption spectra were measured from thylakoid membrane extracts.  
657 Prior to measurement, the samples were placed in darkness in an ice bath to avoid thermal  
658 breakdown of thylakoid structure. Absorbance spectra of all extracts were scanned  
659 spectrophotometrically from 400 to 750 nm with a Shimadzu UV-1800 UV-visible  
660 spectrophotometer. The resuspension buffer was used as a blank and for baseline calibration.

661

### 662 ***In vivo* fluorescence excitation**

663 *In vivo* fluorescence excitation spectra (400-700 nm) were measured as described previously using a  
664 Hitachi F-3000 spectrofluorometer (Nymark et al., 2013). Spectra were obtained by recording the  
665 Chl *a* fluorescence intensity (Chl *a* fluorescence from PSII) at 1 nm spectral resolution (5 nm  
666 bandwidth) at a fixed wavelength of emission (730 nm, 5 nm bandwidth). The emission of light  
667 was measured as a function of absorbed light at different wavelengths for ML acclimated cultures.  
668 All spectra were normalized to the red emission maximum of Chl *a* of the WT cultures, so as to  
669 study the differences in excitation energy transfer efficiency (ETE) by the main photosynthetic

670 pigments Chl *a*, Chl *c* and Fx in the blue-green part of the PAR spectrum, where they exhibit their  
671 maximum absorption.

672

### 673 **77 K chlorophyll fluorescence emission measurements**

674 Low-temperature fluorescence emission spectra were recorded for three biological replicates of ML  
675 acclimated cell cultures using a custom-made 77 K fluorometer (Lamb et al., 2015).  
676 Monochromatic LEDs with an emission centered around either 435 nm (LED435-12-30, Roithner  
677 LaserTechnik) or 470 nm (LED470 Roithner LaserTechnik) were used as excitation  
678 wavelengths. Fluorescence emission spectra were recorded between 600 and 800 nm. Samples were  
679 adjusted to a Chl concentration of 1 µg/mL, transferred to glass tubes and frozen in liquid nitrogen  
680 before measuring the 77 K fluorescence emission. All spectra were normalized to the WT emission  
681 spectrum at 710 nm.

682

### 683 **Protein isolation, SDS-PAGE and Western blot analysis**

684 WT and *alb3b* mutant cultures acclimated to either LL or ML (three biological replicates for each  
685 line and light condition) were harvested by filtration (Durapore Membrane Filters, pore size 0.65  
686 µm; Merck Millipore). Filters were transferred to 2 ml tubes (Sarstedt) and 1 ml F/2 medium was  
687 added. The tubes were vortexed for 10 s for resuspension of the cells, before removal of filters and  
688 centrifugation of re-suspended cells at 16000 *g* for 1 min at 15 °C. The supernatant was removed  
689 and the remaining pellet was flash frozen in liquid nitrogen and stored at -80 °C. A five mm pre-  
690 cooled stainless-steel bead (QIAGEN) was added to each of the tubes with frozen cell pellets, and  
691 the cells were mechanically broken and homogenized in two steps using the TissueLyser system  
692 (QIAGEN). The samples were first placed in a precooled (-80 °C) adapter set followed by cell  
693 disruption for 2 min at 25 Hz. Before the second shaking step (8 min at 25 Hz), the samples were  
694 transferred to a room temperature (RT) adapter set and 700 µl lysis buffer (50 mM Tris, pH 6.8,  
695 2% SDS) were added according to Juhas et al. (Juhas et al., 2014). Insoluble material was removed  
696 by centrifugation (100 *g* for 30 min at 4 °C). The supernatant was transferred to new tubes and the  
697 protein concentration was determined using the DC Protein Assay kit (BioRad) following the  
698 manufacturer's instructions. In addition to the whole cell extracts, lysates were also obtained from  
699 thylakoids isolated from cell cultures acclimated to either LL or ML conditions. Thylakoids were



700 resuspended in lysis buffer (50 mM Tris, pH 6.8, 2% (w/v) SDS) and protein extracts were  
701 obtained as above (the first step for cell breakage was omitted). Proteins were resolved on 12% or  
702 15% SDS-PAGE gels, depending of the size of the protein of interest. 10 µg of the protein  
703 extracts were loaded onto the gel lanes. Western blot analyses were performed on either total  
704 protein extracts (detection of LHCF and LHCX proteins) or thylakoid extracts (detection of D1, D2  
705 and PsaC proteins). The PsaC antibodies produced a signal only when using thylakoid extracts,  
706 whereas the antibody recognizing LHCX proteins produced optimal results when using whole cell  
707 extracts. LHC proteins and photosystem subunits were therefore analyzed in different extracts. The  
708 signal generated by AtpB polyclonal antibodies was used as loading controls on each blot, in  
709 addition to Coomassie stained gels that were run in parallel. 10 µg of the protein extracts were  
710 loaded onto the gels. Proteins were detected with the following antibodies: anti-D1 (AS05 084  
711 Agrisera; 1:20000), anti-D2 (AS06 146 Agrisera; 1:5000), anti-PsaC (AS10 939 Agrisera; 1:1000),  
712 anti-AtpB (AS05 085, Agrisera; 1:4000), anti-LHCF1-11 (1:1000) and anti-FCP6 (LHCX; 1:1000)  
713 (kind gifts from C. Büchel, University of Frankfurt, Germany (Juhás et al., 2014)). Primary  
714 antibody incubation was performed overnight at 4°C for all antibodies. Polyclonal Goat Anti-  
715 Rabbit Immunoglobulins/Biotinylated (Dako) was used as secondary antibody with an incubation  
716 time of 2 h in RT, followed by incubation with Horseradish Peroxidase Streptavidin (Vector  
717 Laboratories) for 1 h also in RT. Protein-antibody cross-reactions were visualized with SuperSignal  
718 West Pico PLUS Chemiluminescent Substrate (Thermo Scientific) and documented with a G:BOX  
719 ChemiXRQ gel doc system (Syngene).

720

### 721 **Transmission electron microscopy**

722 Electron microscopy was used to examine the status of the thylakoid architecture in the *alb3b*  
723 mutant lines. WT and *alb3b-14* cell cultures acclimated to LL were harvested by a light  
724 centrifugation step (4000 g for 10 min) and fixated over night at room temperature in a F/2 medium  
725 buffer containing 2.5% Glutaraldehyde and 2% paraformaldehyde. Pellets were washed three times  
726 in F/2 medium buffer solution and embedded in a 5% gelatin solution. After post-fixation in 2%  
727 osmiumtetroxide and 1.5% kaliumferrocyanid the samples were dehydrated in a gradient of  
728 ethanol. Samples were thereafter embedded with epoxy resins based on Bozzola and Russell's  
729 protocol (Bozzola and Russell, 1999) and sectioned with an ultramicrotome. Images were taken using a  
730 Tecnai 12 transmission electron microscope operating at 80KV. Images were captured using a  
731 MORADA CCD camera.

732

### 733 **Measurements of malondialdehyde content**

734 The malondialdehyde (MDA) content was determined using the Lipid Peroxidation (MDA) assay  
735 kit (Sigma-Aldrich). The MDA concentration was measured based on its reaction with  
736 thiobarbituric acid (TBA) and used as an index of lipid peroxidation. WT, *alb3b* (*alb3b-14*, *alb3b-*  
737 *19*) mutant cultures (three biological replicates for each line) acclimated to HL were harvested by  
738 filtration as described above. The cell pellet was resuspended in the MDA lysis buffer. To ensure  
739 complete lysis the cells were briefly sonicated. Thereafter, the MDA content was determined based  
740 on the manufacturer's instructions. In parallel samples were collected and manually counted to  
741 determine cell concentration.

742

### 743 **Isolation of total RNA and quantitative real-time PCR**

744 Three biological replicates of LL-acclimated WT and *alb3b* mutant cultures were harvested for  
745 isolation of total RNA in parallel to the samples harvested for protein analyses as described above.  
746 Total RNA isolation, quantification and verification of RNA integrity were performed as described  
747 in Nymark et al. (Nymark et al., 2009). Reverse transcription of RNA was performed with the  
748 QuantiTect Reverse Transcription kit (Qiagen) following the recommended protocol. 1 µg of total  
749 RNA was used in each reaction. Quantitative real-time PCR (qRT-PCR) analysis were performed as  
750 described in Nymark et al. (Nymark et al., 2009) for calculation of relative expression ratios of four  
751 *LHCF* genes (*LHCF1*, *LHCF2*, *LHCF5* and *LHCF8*). The geNorm module in the qBasePLUS  
752 software (Biogazelle) was used for determining the expression stability of candidate reference gene.  
753 Based on the stability analysis *RPS5* (Phatr2\_42848) and *DLST* (Phatr2\_45557) were picked as  
754 reference genes (Nymark et al., 2013; Valle et al., 2014). LinRegPCR software (Ramakers et al.,  
755 2003; Ruijter et al., 2009) was used to calculate mean PCR efficiency per amplicon and cycle  
756 threshold (Ct) values per sample. These data were imported into the qBasePLUS software  
757 (Biogazelle), which calculated relative expression ratios (given as Calibrated Normalized Relative  
758 Quantities (CNRQ)) and performed statistical analyses on the results. The one-way ANOVA test  
759 integrated in the qBasePLUS software was used to evaluate the significance of the estimated  
760 relative expression ratios. Forward and reverse primers are listed in Supplementary Table S5.

761

### 762 **Light shift time-series experiments**

763 LL acclimated WT and *alb3b* KO lines were transferred to ML conditions and sampled after 0.5, 6,  
764 24, 48 and 168 h following the shift in growth light intensity. LL samples (0 h) were harvested as  
765 controls. Three biological replicates were set up for each line and time point to reach a cell  
766 concentration of maximum  $1 \times 10^6$  cells/mL at the day of harvesting. Samples were harvested for  
767 pigment analyses, monitoring of cell concentrations, variable *in vivo* Chl *a* fluorescence (PAM), and  
768 protein analyses.

769

## 770 **Pigment analyses**

771 The HPLC pigment analysis was performed according to Rodriguez et al. (Rodriguez et al., 2006)  
772 using a Hewlett-Packard HPLC 1100 Series system. Pigment values from the HPLC analysis were  
773 calculated as fmol pigment per cell. Cell numbers were calculated from flow cytometer counts as  
774 described above.

775

## 776 **Measurements of photosynthetic parameters**

777 A PhytoPAM (System I, Walz, Germany) was used to measure variable Chl *a* fluorescence of the  
778 harvested samples. The photosynthesis *vs.* irradiance relationship was obtained as described  
779 previously (Nymark et al., 2009). An additional step at  $1216 \mu\text{mol photons m}^{-2} \text{s}^{-1}$  was added for the  
780 samples that had been treated with ML for 1 week to ensure that light saturation levels were  
781 reached. The maximum quantum yield of PSII ( $F_v/F_m$ ), the maximum relative electron transport  
782 rate ( $rETR_{\text{max}}$ ), the maximum light utilization coefficient ( $\alpha$ ) and the light saturation index ( $E_k$ ) were  
783 calculated as described before (Nymark et al., 2009). The  $rETR_{\text{max}}$  is an estimate of the maximum  
784 photosynthetic capacity of the cells ( $\sim P_{\text{max}}$ ), whereas the light saturation index  $E_k$  ( $rETR_{\text{max}}/\alpha$ ) is a  
785 proxy for the threshold irradiance that separates light-limited and light-saturated photosynthesis  
786 (Genty et al., 1989; Sakshaug et al., 1997).  $F_m$  at low light intensities is commonly observed to be  
787 lower than the  $F_m'$  level under low actinic light in diatoms (Serôdio et al., 2006; Cruz and Serôdio,  
788 2008; Cruz et al., 2011). NPQ was therefore calculated from the light-response curve from LL  
789 acclimated samples, using the maximum  $F_m'$  level ( $F_m'_{\text{max}}$ ) instead of  $F_m$  as follows:  $\text{NPQ} =$   
790  $(F_m'_{\text{max}}/ F_m') - 1$  (Serôdio et al., 2006; Kalaji et al., 2017). NPQ development over time was  
791 additionally calculated from LL acclimated cells exposed to 5 min of actinic light at an intensity  
792 setting of  $832 \mu\text{mol photons m}^{-2} \text{s}^{-1}$ . For the HL experiment,  $F_v/F_m$  was measured with an AquaPen-  
793 C (Photon System Instruments) at the end of a 30 min dark acclimation period to relax the fast-

794 reversible component (qE) of NPQ so that only the photoinhibitory slowly reversible quenching  
795 (qI), caused by damaged PSII reaction centers, would influence the  $F_v/F_m$  value.

796 Oxygen evolution was measured at 15 °C using a S1 Clark Type polarographic oxygen electrode  
797 (Hansatech) increasingly illuminated with a 35 W cool white spot LED. The measurements were  
798 done on cultures acclimated both to LL and ML. 2 ml cell suspension from mid-exponential phase  
799 culture was added to a stirred chamber with temperature control and supplemented with sodium  
800 bicarbonate (30 µl of a 0.5 M solution) so that the oxygen production would not be limited by  
801 carbon availability. Prior to measuring, the Chl *a* concentration in the sample was adjusted to a  
802 concentration lower than 1.2 µM to avoid cell shading in the chamber. Simultaneously, cell  
803 concentration of the samples was determined by Flow cytometry counting. Oxygen consumption in  
804 darkness was measured as a starting baseline, thereafter the sample was exposed to gradually  
805 increasing light intensities and the oxygen evolution was measured continuously for at least 10 min.  
806 Each light intensity was adjusted by measuring the light intensity in the middle of the electrode  
807 chamber with a spherical US-SQS sensor (Waltz).

808

### 809 **Complementation of *alb3b* KO lines**

810 A modified version of the *ALB3b* gene was synthesized together with its native promoter by  
811 GeneArt® Services Thermo Fisher Scientific Inc (Supplementary Figure S16). Modifications  
812 consisted of changes of the codon usage in the PAM and target region of the *ALB3b* gene to avoid  
813 gene editing by the functional CRISPR/Cas9 system incorporated into the genome of the *alb3b* KO  
814 lines. MssI sites were included at the 5' and 3' ends of the module to facilitate blunt-end cloning  
815 into the pM9\_4Compln vector from Madhuri et al. (Madhuri et al., 2019) containing the *bsr* gene  
816 conferring resistance to blasticidin-S. Transformation of all three *alb3b* KO lines with the  
817 pM9\_4Compln vector containing the synthesized *ALB3b* module was performed as described  
818 previously (Nymark et al., 2017). The algae were transferred to low-salt selection plates (25% (v/v)  
819 natural seawater supplemented with f/2-Si, 1% (w/v) agar, 4 µg/mL blasticidin-S (Thermo Fisher  
820 Scientific)) ~ 24 h after transformation. Transformed colonies appeared 3-4 weeks after transfer to  
821 selection plates. Colonies that had regained the normal brown color were randomly picked from the  
822 selection plates. PCR amplification of the *ALB3b* gene and subsequent sequencing were used to test  
823 for the presence of the modified version of the *ALB3b* gene (and the absence of WT sequence).

824 Primers used for both PCR amplification and sequencing were PtAlb3b-G1F and PtAlb3b-G1R  
825 (Supplementary Table S5). One complemented *alb3b* colony, resulting from each of the  
826 transformations performed with the *alb3b* KO lines, was cultivated for pigment and protein  
827 analyses, as described above.

828

829

### 830 **ACCESSION NUMBERS:**

831 Accession numbers for ALBINO protein sequences extracted from GenBank NCBI, the iMicrobe  
832 database (Marine Microbial Eukaryote Transcriptome Sequencing Project (MMETSP)) and from  
833 the JGI genome portal are listed in Supplementary Table S4.

834

### 835 **SUPPLEMENTAL DATA:**

836 **Supplemental Figure 1:** Phylogenetic relationship between members of the ALBINO3 family.

837 **Supplemental Figure 2:** C-terminal domain of diatom ALB3a and ALB3b proteins.

838 **Supplemental Figure 3:** DNA sequences for the *ALB3b* WT gene and the inserts in the *alb3b* KO  
839 lines.

840 **Supplemental Figure 4:** Allele-specific amplification of the Cas9 target site within the *ALB3b*  
841 gene in WT and *alb3b* mutant strains.

842 **Supplemental Figure 5.** Relative expression levels of LHCF genes in *alb3b* lines compared to WT.

843 **Supplemental Figure 6.** Transmission electron micrographs of WT and *alb3b-14* mutant line cells.

844 **Supplementary Figure 7.** NPQ development over time in WT and *alb3b* lines.

845 **Supplemental Figure 8.** Western blot analysis of LHCF and LHCX proteins from WT and *alb3b*  
846 mutant lines.

847 **Supplemental Figure 9.** Re-evaluation of pigment concentration per cell for WT and *alb3b*  
848 mutants at LL.

849 **Supplemental Figure 10.** Re-evaluation of photo-physiological responses of LL-acclimated WT  
850 and *alb3b* mutant lines.

851 **Supplemental Figure 11.** Light-saturation curves of photosynthesis for LL and ML-acclimated WT  
852 and *alb3b* mutant lines presented as oxygen evolution per cell.

853 **Supplemental Figure 12:** Growth curves for WT and *alb3b* mutants.

854 **Supplemental Figure 13:** Growth curves and corresponding measurements of photosynthetic  
855 efficiency of WT and *alb3b* mutants in high light.

856 **Supplemental Figure 14:** Malondialdehyde (MDA) product of lipid peroxidation.

857 **Supplemental Figure 15:** PCR analysis and Sanger sequencing of PCR products from  
858 complemented *alb3b* lines.

859 **Supplemental Figure 16:** DNA sequence representing the synthetic *ALB3b* module used for  
860 complementation of the *alb3b* KO lines.

861 **Supplemental Table 1:** Cycle threshold (Ct) values for LHCF and reference genes

862 **Supplemental Table 2:** Fraction of Chl *a* and Fx content in *alb3b* mutant lines compared to WT in  
863 LL (0h) and after 0.5-168 h in ML.

864 **Supplemental Table 3:** Oxygen evolution values of the light-saturation curves of photosynthesis  
865 including St.Dev. for LL and ML-acclimated WT and *alb3b* mutant lines.

866 **Supplemental Table 4:** Accession numbers for ALBINO proteins included in the phylogenetic  
867 analyses.

868 **Supplemental Table 5:** Oligo and primer sequences.

869

## 870 **ACKNOWLEDGEMENTS:**

871 We wish to thank Professor Claudia Büchel for kindly providing LHCF and LHCX antibodies and  
872 Professor Peter Kroth for the pM9\_4Compln vector. The authors would also like to thank Kjersti  
873 Andresen for assistance with the HPLC analyses, Professor Geir Johnsen and Inga Aamot for access

874 to and guidance on use of the PhytoPAM, and Associate professor Martin F. Hohmann-Marriot and  
 875 Gunvor Røkke for training on how to produce and analyze 77 K data. The authors would like to  
 876 thank the Cellular and Molecular Imaging Core Facility (CMIC), Norwegian University of Science  
 877 and Technology (NTNU) for guidance and help during the acquisition of the TEM images. CMIC is  
 878 funded by the Faculty of Medicine at NTNU and Central Norway Regional Health Authority.

879

880 **TABLES:**

881

882 **Table 1. Photosystem absorption cross-section and Chl *a* content per P700 in *alb3b* mutants**  
 883 **compared to WT cells.** Photosystem absorption cross-section was measured as rate of 533 nm  
 884 (Fx) or 670 nm (Chl *a*) photons absorbed by the functional thylakoid membranes. The actinic light  
 885 intensity was adjusted to  $I_{670} = 2.1 \mu\text{mol photons m}^{-2} \text{s}^{-1}$  and  $I_{533} = 12 \mu\text{mol photons m}^{-2} \text{s}^{-1}$ . Rates  
 886 of light absorption and utilization are given in photons per second with  $\pm$ SD. P700 quantification  
 887 was measured from the light induced  $\Delta A_{700}$  with 670 nm (Chl *a*) actinic illumination.

888

		<i>WT</i>	<i>alb3b-14</i>	<i>alb3b-16</i>	<i>alb3b-19</i>	Average <i>alb3b</i>	<i>alb3b</i> /WT %
PSI	(Fx) 533 nm	$2.61 \text{ s}^{-1} \pm 0.40$	$1.10 \pm 0.08$	$1.17 \pm 0.10$	$1.09 \pm 0.00$	$1.10 \pm 0.06 \text{ s}^{-1}$	42 %
	(Chl) 670 nm	$1.93 \text{ s}^{-1} \pm 0.11$	$1.43 \pm 0.05$	$1.39 \pm 0.15$	$1.39 \pm 0.14$	$1.40 \pm 0.01 \text{ s}^{-1}$	72.5%
PSII	(Fx) 533 nm	$32.30 \text{ s}^{-1} \pm 0.7$	$13.92 \pm 1.96$	$8.10 \pm 1.16$	$8.58 \pm 0.93$	$10.17 \pm 3.24 \text{ s}^{-1}$	35 %
	(Chl) 670 nm	$12.62 \text{ s}^{-1} \pm 2.69$	$7.21 \pm 0.00$	$7.08 \pm 0.90$	$6.71 \pm 1.36$	$7.00 \pm 0.26 \text{ s}^{-1}$	55 %
Chl <i>a</i> /P700		663 $\pm$ 9 % : 1	466 $\pm$ 11 %	414 $\pm$ 9 %	394 $\pm$ 11 %	425:1	64%

889

890

891 **Table 2. Photosynthesis and respiration properties of the WT and the *alb3b* KO lines.**  
 892 Parameters are calculated from the light-saturation curves of photosynthesis based on oxygen  
 893 evolution of WT and *alb3b* KO lines (Figure 7; LL: Figure 7E, ML: Figure7F). Data for *alb3b* are  
 894 presented as an average of the three independent *alb3b* KO (*alb3b-14*, *alb3b-16*, *alb3b-19*) lines  
 895  $\pm$ SD. A minimum of three biological replicates were measured for each independent line.  
 896

	LL		ML	
	WT	<i>alb3b</i>	WT	<i>alb3b</i>
<b>Respiration (<math>\mu\text{mol O}_2/\text{mol Chl/s}</math>)</b>	30.0 $\pm$ 13.6	23.8 $\pm$ 1.7	23.5 $\pm$ 5.9	24.9 $\pm$ 3.2
<b>P<sub>max</sub> (<math>\mu\text{mol O}_2/\text{mol Chl/s}</math>)</b>	57.7 $\pm$ 11.5	63.2 $\pm$ 3.1	55.7 $\pm$ 4.9	71.8 $\pm$ 7.6
<b>E<sub>s</sub>(Saturation intensity, <math>\mu\text{mol photons m}^{-2}\text{s}^{-1}</math>)</b>	96.5	250	170	> 400
<b>Maximum light utilization coefficient (<math>\alpha</math>)</b>	0.35	0.32	0.29	0.25

897  
898

899 **Table 3. Growth rates of WT and *alb3b* mutant lines acclimated to different light intensities.**  
 900 Maximum cell division per day were calculated from three biological replicates of WT and *alb3b*  
 901 KO lines acclimated to LL (35  $\mu\text{mol photons m}^{-2}\text{s}^{-1}$ ), ML (200  $\mu\text{mol photons m}^{-2}\text{s}^{-1}$ ) or HL (480  
 902  $\mu\text{mol photons m}^{-2}\text{s}^{-1}$ ). Values are presented with  $\pm$ SD. Growth rate for the *alb3b-16* mutant in HL  
 903 was not calculated because of cell aggregation.

	WT	<i>alb3b-14</i>	<i>alb3b-16</i>	<i>alb3b-19</i>	<i>alb3b</i> average
<b>LL</b>	1.6 $\pm$ 0.23	0.4 $\pm$ 0.02	0.6 $\pm$ 0.02	0.6 $\pm$ 0.03	0.5 $\pm$ 0.09
<b>ML</b>	2.2 $\pm$ 0.03	1.1 $\pm$ 0.01	1.2 $\pm$ 0.03	1.4 $\pm$ 0.05	1.2 $\pm$ 0.13
<b>HL</b>	2.0 $\pm$ 0.05	0.8 $\pm$ 0.17	n/a	0.9 $\pm$ 0.25	0.8 $\pm$ 0.19

904  
905  
906



907

908 **FIGURE LEGENDS:**

909 **Figure 1: Presentation of intact and truncated ALB3b protein.** A) The area of the ALB3b  
910 protein corresponding to the 20 bp target region for CRISPR/Cas9-based gene editing is located  
911 toward the N-terminal part of the protein (blue highlighting) with the PAM site located at the  
912 reverse DNA strand (green highlighting). CTP: Chloroplast targeting peptide; 60 kD IMP: 60 kD  
913 Inner Membrane Protein domain; CTD: conserved C-terminal domain. B) Overview of amino acid  
914 sequences resulting from CRISPR/Cas9 induced inserts in the three *alb3b* KO lines causing  
915 premature stop codons and truncated ALB3b proteins. Color coding: Blue: WT target sequence;  
916 Green: amino acid corresponding to PAM site; Red letters: Insert; \*: Premature stop. C) Protein  
917 alignment based on the C-terminal domain (CTD) of ALB3b proteins in diatoms.

918

919 **Figure 2. Color differences and spectral characteristics of WT and *alb3b* mutants.** A) Visual  
920 representation of the *alb3b* phenotype compared to WT at low light (LL; 35  $\mu\text{mol photons m}^{-2} \text{s}^{-1}$ ;  
921 left side) and ML (200  $\mu\text{mol photons m}^{-2} \text{s}^{-1}$ ; right side). For comparison and visualization of the  
922 color differences, all cultures were adjusted to equal cell densities ( $3 \times 10^7$  cells/ml). B) Absorbance  
923 spectra and C) *in vivo* fluorescence excitation spectra of cultures acclimated to ML. Isolated intact  
924 thylakoid membranes were used for recording of the absorption spectra to avoid scattering.  
925 Fluorescence emission was measured at 730 nm to ensure origin from the reaction center II Chl *a*.  
926 Insets: Difference spectra between: the absorbance of WT and *alb3b* KO lines B) and excitation  
927 energy transfer in the blue-green region of the *in vivo* fluorescence excitation spectra C). WT:  
928 Presented as an average of three biological replicates; *alb3b*: Presented as an average of the three  
929 *alb3b* KO lines 14, 16 and 19 with  $\pm$ SD for all data points indicated by the grey area around the  
930 graphs. Three biological replicates were measured for each line.

931

932 **Figure 3. 77 K fluorescence emission spectra of WT and *alb3b* KO samples acclimated to ML.**  
933 Samples were excited at either A) 435 nm or B) 470 nm. The emission spectra were normalized at  
934 their 710 nm maximum. Data for *alb3b* is an average of the three *alb3b* KO lines 14, 16 and 19  
935 with  $\pm$ SD for all data points indicated by the grey area around the graphs. Three biological

936 replicates were measured for each line including the WT.

937

938 **Figure 4. Western blot analysis of thylakoid membrane proteins from WT and *alb3b* mutant**  
939 **lines acclimated to low light (LL; 35  $\mu\text{mol photons m}^{-2} \text{s}^{-1}$ ) or medium light (ML; 200  $\mu\text{mol}$**   
940 **photons  $\text{m}^{-2} \text{s}^{-1}$ ) conditions.** A) Abundance of LHC proteins belonging to the LHCF group were  
941 evaluated using an antibody recognizing LHCF1-11, whereas the LHCX proteins were recognized  
942 by anti-FCP6 (a LHCX family member of *C. meneghiniana*). A dilution series of the WT samples  
943 were used to assess the level of LHC proteins in *alb3b* mutants compared to WT. B) Protein  
944 expression of PSII and PSI core proteins were evaluated with antibodies against the D1 (PSII), D2  
945 (PSII) and PsaC (PSI) core subunits. A dilution series of the *alb3b* samples were used to assess the  
946 level of photosystem subunits in *alb3b* mutants compared to WT. An antibody recognizing the  $\beta$ -  
947 subunit of ATP synthase (AtpB) were used as loading control on each of the individual blots. Lanes  
948 marked with 100% contain 10  $\mu\text{g}$  (20  $\mu\text{g}$  for analysis of LHCX levels) of protein extracts.  
949 Images have been cropped.

950

951 **Figure 5. Pigment concentrations per cell for WT and *alb3b* mutant lines as a function of ML**  
952 **exposure time.** Cellular pigment concentrations of A) Chl *a*, B) Fx, C) Ddx and D) Dtx in WT and  
953 *alb3b* mutant cells as a function of time following a shift from LL conditions (0 h; 35  $\mu\text{mol photons}$   
954  $\text{m}^{-2} \text{s}^{-1}$ ) to ML conditions (200  $\mu\text{mol photons m}^{-2} \text{s}^{-1}$ ) for 0.5, 6, 24, 48 and 168 h. Results are  
955 presented as a mean of three biological replicates with  $\pm\text{SD}$ .

956

957 **Figure 6. De-epoxidation state index and NPQ capacity of WT and *alb3b* mutants.** A) De-  
958 epoxidation state index ( $\text{DES} = \text{Dtx}/(\text{Dtx} + \text{Ddx})$ ) calculated from the HPLC pigment data from LL  
959 acclimated (0 h) WT and *alb3b* cultures exposed to ML for 0.5, 6, 24, 48 and 168 h. B) Capacity for  
960 NPQ calculated from rapid light curves derived from LL acclimated cells approx. two months after  
961 isolation of mutated single cells and C) after being maintained in culture for one more year.  $\text{NPQ} =$   
962  $(F_{m'}^{\text{max}}/F_{m'}) - 1$ .  $F_{m'}^{\text{max}}$  replaces the commonly used  $F_m$  since  $F_{m'}$  values frequently occur that are  
963 higher than the  $F_m$  from dark-treated diatom samples (Serôdio et al., 2006). Results are presented as  
964 a mean of three biological replicates with  $\pm\text{SD}$ .

965

966 **Figure 7. Photo-physiological responses of WT and *alb3b* mutant lines. *In vivo* Chl *a***

967 fluorescence kinetics (PAM) were used to estimate A) the maximum quantum yield of PSII ( $F_v/F_m$ ),  
968 B) the maximum light utilization coefficient ( $\alpha$ ), C) the maximum relative light-saturated electron  
969 transport rate ( $rETR_{max}$ ) and D) the light saturation index ( $E_k$ ) in LL (0h) acclimated WT and *alb3b*  
970 KO lines as a function of ML exposure time (0.5-168 h). Values are presented with  $\pm$ SD bars.  
971 Light-saturation curves of photosynthesis based on oxygen evolution were produced for E) LL  
972 acclimated and F) ML acclimated WT and *alb3b* KO lines. The oxygen concentration was  
973 normalized on a per-Chl basis. The results were fit with curves based on a polynomial regression  
974 using R. All values are presented as an average of three biological replicates for each line and  $\pm$ SD  
975 for each value can be found in Supplementary Table S3.

976

977 **Figure 8. Culture color, LHCF protein level and pigment concentration in complemented**  
978 ***alb3b* lines compared to WT.** A) WT and complemented *alb3b* KO lines (*alb3b-14C*, *alb3b-16C*,  
979 *alb3b-19C*) were acclimated to LL and ML conditions. All cultures were concentrated and adjusted  
980 to equal cell densities ( $3 \times 10^7$  cells/ml) for comparison. B) Western blot analysis of LHCF proteins  
981 in WT and complemented *alb3b* mutant lines acclimated to LL and ML conditions. LHCF protein  
982 levels were evaluated using LHCF1-11 antibody. An antibody recognizing the  $\beta$ -subunit of ATP  
983 synthase was used as loading control. 10  $\mu$ g of total protein from cell lysates was loaded onto  
984 the gel. C) Cellular pigment concentrations of Chl *a* and Fx in LL conditions. Results are presented  
985 as a mean of three biological replicates with  $\pm$ SD bars.

986

987 **Figure 9. Proposed model of the role of diatom ALB3 insertases in insertion/assembly of**  
988 **thylakoid membrane proteins.** LHC proteins are synthesized on ribosomes on the cERM,  
989 transported through the four membranes surrounding the secondary plastid of diatoms, and guided  
990 to ALB3b by an unknown protein complex before incorporation into the thylakoid membrane (left  
991 side). Chloroplast-encoded proteins are suggested to be integrated by the co-translational cpSRP  
992 pathway including cpSRP54, FTSY and ALB3ba (right side). cERM: chloroplast ER membrane;  
993 PPM: periplastidal membrane; OEM: plastid outer envelope membrane; IEM: plastid inner  
994 envelope membrane. CpSRP54: chloroplast signal recognition particle protein 54; CpFTSY:  
995 chloroplast SRP receptor; ALB3: chloroplast SRP insertase Albino3.

996

997

998

999 **REFERENCES**

- 1000 **Ago H, Adachi H, Umena Y, Tashiro T, Kawakami K, Kamiya N, Tian L, Han G, Kuang T,**  
1001 **Liu Z, Wang F, Zou H, Enami I, Miyano M, Shen JR** (2016) Novel features of  
1002 eukaryotic photosystem II revealed by its crystal structure analysis from a red alga. *J Biol*  
1003 *Chem* **291**: 5676-5687
- 1004 **Armbrust EV, Berges JA, Bowler C, Green BR, Martinez D, Putnam NH, Zhou S, Allen AE,**  
1005 **Apt KE, Bechner M, Brzezinski MA, Chaal BK, Chiovitti A, Davis AK, Demarest MS,**  
1006 **Detter JC, Glavina T, Goodstein D, Hadi MZ, Hellsten U, Hildebrand M, Jenkins BD,**  
1007 **Jurka J, Kapitonov VV, Kroger N, Lau WW, Lane TW, Larimer FW, Lippmeier JC,**  
1008 **Lucas S, Medina M, Montsant A, Obornik M, Parker MS, Palenik B, Pazour GJ,**  
1009 **Richardson PM, Rynearson TA, Saito MA, Schwartz DC, Thamtracoln K, Valentin**  
1010 **K, Vardi A, Wilkerson FP, Rokhsar DS** (2004) The genome of the diatom *Thalassiosira*  
1011 *pseudonana*: ecology, evolution, and metabolism. *Science* **306**: 79-86
- 1012 **Austin JR, 2nd, Staehelin LA** (2011) Three-dimensional architecture of grana and stroma  
1013 thylakoids of higher plants as determined by electron tomography. *Plant Physiol* **155**: 1601-  
1014 1611
- 1015 **Bailleul B, Rogato A, de Martino A, Coesel S, Cardol P, Bowler C, Falciatore A, Finazzi G**  
1016 (2010) An atypical member of the light-harvesting complex stress-related protein family  
1017 modulates diatom responses to light. *Proc Natl Acad Sci U S A* **107**: 18214-18219
- 1018 **Baroli I, Melis A** (1996) Photoinhibition and repair in *Dunaliella salina* acclimated to different  
1019 growth irradiances. *Planta* **198**: 640-646
- 1020 **Bellafiore S, Ferris P, Naver H, Gohre V, Rochaix JD** (2002) Loss of Albino3 leads to the  
1021 specific depletion of the light-harvesting system. *Plant Cell* **14**: 2303-2314
- 1022 **Ben-Shem A, Frolow F, Nelson N** (2003) Crystal structure of plant photosystem I. *Nature* **426**:  
1023 630-635
- 1024 **Bowler C, Allen AE, Badger JH, Grimwood J, Jabbari K, Kuo A, Maheswari U, Martens C,**  
1025 **Maumus F, Otiillar RP, Rayko E, Salamov A, Vandepoele K, Beszteri B, Gruber A,**  
1026 **Heijde M, Katinka M, Mock T, Valentin K, Verret F, Berges JA, Brownlee C, Cadoret**  
1027 **JP, Chiovitti A, Choi CJ, Coesel S, De Martino A, Detter JC, Durkin C, Falciatore A,**  
1028 **Fournet J, Haruta M, Huysman MJ, Jenkins BD, Jiroutova K, Jorgensen RE, Joubert**  
1029 **Y, Kaplan A, Kroger N, Kroth PG, La Roche J, Lindquist E, Lommer M, Martin-**  
1030 **Jezequel V, Lopez PJ, Lucas S, Mangogna M, McGinnis K, Medlin LK, Montsant A,**  
1031 **Oudot-Le Secq MP, Napoli C, Obornik M, Parker MS, Petit JL, Porcel BM, Poulsen**  
1032 **N, Robison M, Rychlewski L, Rynearson TA, Schmutz J, Shapiro H, Siat M, Stanley**  
1033 **M, Sussman MR, Taylor AR, Vardi A, von Dassow P, Vyverman W, Willis A, Wyrwicz**  
1034 **LS, Rokhsar DS, Weissenbach J, Armbrust EV, Green BR, Van de Peer Y, Grigoriev**  
1035 **IV** (2008) The *Phaeodactylum* genome reveals the evolutionary history of diatom genomes.  
1036 *Nature* **456**: 239-244
- 1037 **Bozzola JJ, Russell LD** (1999) *Electron Microscopy: Principles and Techniques for Biologists*, Ed  
1038 2. Jones and Bartlett, Boston
- 1039 **Bricaud A, Claustre H, Ras J, Oubelkheir K** (2004) Natural variability of phytoplanktonic  
1040 absorption in oceanic waters: Influence of the size structure of algal populations. *J Geophys*  
1041 *Res-Oceans* **109**
- 1042 **Brown JW, Sorhannus U** (2010) A molecular genetic timescale for the diversification of

- 1043 autotrophic stramenopiles (Ochrophyta): substantive underestimation of putative fossil ages.  
1044 PLoS One **5**
- 1045 **Büchel C** (2014) Fucoxanthin-Chlorophyll-proteins and non-photochemical fluorescence  
1046 quenching of diatoms. In B Demmig-Adams, G Garab, W Adams III, Govindjee, eds, Non-  
1047 photochemical quenching and energy dissipation in plants, algae and cyanobacteria.  
1048 Advances in photosynthesis and respiration (Including bioenergy and related processes), Vol  
1049 40. Springer, Dordrecht
- 1050 **Büchel C** (2015) Evolution and function of light harvesting proteins. J Plant Physiol **172**: 62-75
- 1051 **Chandrasekar S, Shan SO** (2017) Anionic phospholipids and the Albino3 translocase activate  
1052 signal recognition particle-receptor interaction during light-harvesting chlorophyll *a/b*-  
1053 binding protein targeting. J Biol Chem **292**: 397-406
- 1054 **Cruz S, Goss R, Wilhelm C, Leegood R, Horton P, Jakob T** (2011) Impact of chlororespiration  
1055 on non-photochemical quenching of chlorophyll fluorescence and on the regulation of the  
1056 diadinoxanthin cycle in the diatom *Thalassiosira pseudonana*. J Exp Bot **62**: 509-519
- 1057 **Cruz S, Serôdio J** (2008) Relationship of rapid light curves of variable fluorescence to  
1058 photoacclimation and non-photochemical quenching in a benthic diatom. Aquat Bot **88**:  
1059 256-264
- 1060 **De Martino A, Bartual A, Willis A, Meichenin A, Villazan B, Maheswari U, Bowler C** (2011)  
1061 Physiological and molecular evidence that environmental changes elicit morphological  
1062 interconversion in the model diatom *Phaeodactylum tricornutum*. Protist **162**: 462-481
- 1063 **De Martino A, Meichenin A, Shi J, Pan KH, Bowler C** (2007) Genetic and phenotypic  
1064 characterization of *Phaeodactylum tricornutum* (Bacillariophyceae) accessions. J Phycol **43**:  
1065 992-1009
- 1066 **Durnford DG, Aebersold R, Green BR** (1996) The fucoxanthin-chlorophyll proteins from a  
1067 chromophyte alga are part of a large multigene family: structural and evolutionary  
1068 relationships to other light harvesting antennae. Mol Gen Genet **253**: 377-386
- 1069 **Dünschede B, Bals T, Funke S, Schunemann D** (2011) Interaction studies between the chloroplast  
1070 signal recognition particle subunit cpSRP43 and the full-length translocase Alb3 reveal a  
1071 membrane-embedded binding region in Alb3 protein. J Biol Chem **286**: 35187-35195
- 1072 **Falk S, Ravaud S, Koch J, Sinning I** (2010) The C terminus of the Alb3 membrane insertase  
1073 recruits cpSRP43 to the thylakoid membrane. J Biol Chem **285**: 5954-5962
- 1074 **Falk S, Sinning I** (2010) The C terminus of Alb3 interacts with the chromodomains 2 and 3 of  
1075 cpSRP43. J Biol Chem **285**: 1e25-26; author reply 1e26-28
- 1076 **Falkowski PG, Barber RT, Smetacek V** (1998) Biogeochemical controls and feedbacks on ocean  
1077 primary production. Science **281**: 200-206
- 1078 **Falkowski PG, Raven JA** (2007) Aquatic photosynthesis, Ed Second edition. Princeton University  
1079 Press, Princeton
- 1080 **Fawley MW** (1984) Effects of light intensity and temperature interactions on growth  
1081 characteristics of *Phaeodactylum tricornutum* (Bacillariophyceae). J Phycol **20**: 67-72
- 1082 **Formighieri C, Melis A** (2017) Heterologous synthesis of geranylinalool, a diterpenol plant  
1083 product, in the cyanobacterium *Synechocystis*. Appl Microbiol Biotechnol **101**: 2791-2800
- 1084 **Genty B, Briantais JM, Baker NR** (1989) The relationship between the quantum yield of  
1085 photosynthetic electron-transport and quenching of chlorophyll fluorescence. Biochim  
1086 Biophys Acta **990**: 87-92
- 1087 **Gerdes L, Bals T, Klostermann E, Karl M, Philippar K, Hunken M, Soll J, Schunemann D**  
1088 (2006) A second thylakoid membrane-localized Alb3/OxaI/YidC homologue is involved in  
1089 proper chloroplast biogenesis in *Arabidopsis thaliana*. J Biol Chem **281**: 16632-16642

- 1090 **Giovagnetti V, Ruban AV** (2017) Detachment of the fucoxanthin chlorophyll *a/c* binding protein  
1091 (FCP) antenna is not involved in the acclimative regulation of photoprotection in the  
1092 pennate diatom *Phaeodactylum tricornutum*. *Biochim Biophys Acta* **1858**: 218-230
- 1093 **Goss R, Lepetit B** (2015) Biodiversity of NPQ. *J Plant Physiol* **172**: 13-32
- 1094 **Grouneva I, Rokka A, Aro EM** (2011) The thylakoid membrane proteome of two marine diatoms  
1095 outlines both diatom-specific and species-specific features of the photosynthetic machinery.  
1096 *J Proteome Res* **10**: 5338-5353
- 1097 **Gu J, Zhou Z, Li Z, Chen Y, Wang Z, Zhang H, Yang J** (2017) Photosynthetic properties and  
1098 potentials for improvement of photosynthesis in pale green leaf rice under high light  
1099 conditions. *Front Plant Sci* **8**: 1082
- 1100 **Guenther JE, Melis A** (1990) The physiological significance of photosystem II heterogeneity in  
1101 chloroplasts. *Photosynth Res* **23**: 105-109
- 1102 **Guillard RR, Ryther JH** (1962) Studies of marine planktonic diatoms. I. *Cyclotella nana* Hustedt,  
1103 and *Detonula confervacea* (Cleve) Gran. *Can J Microbiol* **8**: 229-239
- 1104 **Gundermann K, Büchel C** (2014) Structure and functional heterogeneity of fucoxanthin-  
1105 chlorophyll proteins in diatoms. In M Hohmann-Marriott, ed, *The Structural Basis of*  
1106 *Biological Energy Generation. Advances in Photosynthesis and Respiration (Including*  
1107 *Bioenergy and Related Processes)*, Vol 39. Springer Dordrecht
- 1108 **Göhre V, Ossenbuhl F, Crevecoeur M, Eichacker LA, Rochaix JD** (2006) One of two alb3  
1109 proteins is essential for the assembly of the photosystems and for cell survival in  
1110 *Chlamydomonas*. *Plant Cell* **18**: 1454-1466
- 1111 **Havaux M, Dall'Osto L, Bassi R** (2007) Zeaxanthin has enhanced antioxidant capacity with  
1112 respect to all other xanthophylls in *Arabidopsis* leaves and functions independent of binding  
1113 to PSII antennae. *Plant Physiol* **145**: 1506-1520
- 1114 **Hennon SW, Soman R, Zhu L, Dalbey RE** (2015) YidC/Alb3/Oxa1 family of insertases. *J Biol*  
1115 *Chem* **290**: 14866-14874
- 1116 **Herbstova M, Bina D, Kana R, Vacha F, Litvin R** (2017) Red-light phenotype in a marine  
1117 diatom involves a specialized oligomeric red-shifted antenna and altered cell morphology.  
1118 *Sci Rep* **7**: 11976
- 1119 **Hiyama T, Ke B** (1972) Difference spectra and extinction coefficients of P700. *Biochim Biophys*  
1120 *Acta* **267**: 160-171
- 1121 **Ikeda Y, Komura M, Watanabe M, Minami C, Koike H, Itoh S, Kashino Y, Satoh K** (2008)  
1122 Photosystem I complexes associated with fucoxanthin-chlorophyll-binding proteins from a  
1123 marine centric diatom, *Chaetoceros gracilis*. *Biochim Biophys Acta* **1777**: 351-361
- 1124 **Jeffrey SW, Humphrey GF** (1975) New spectrophotometric equations for determining  
1125 chlorophylls *a*, *b*, *c1* and *c2* in higher plants, algae and natural phytoplankton. *Biochem*  
1126 *Physiol Pfl* **167**: 191-194
- 1127 **Juhas M, Buchel C** (2012) Properties of photosystem I antenna protein complexes of the diatom  
1128 *Cyclotella meneghiniana*. *J Exp Bot* **63**: 3673-3681
- 1129 **Juhas M, von Zadow A, Spexard M, Schmidt M, Kottke T, Buchel C** (2014) A novel  
1130 cryptochrome in the diatom *Phaeodactylum tricornutum* influences the regulation of light-  
1131 harvesting protein levels. *Febs J* **281**: 2299-2311
- 1132 **Kalaji HM, Schansker G, Brestic M, Bussotti F, Calatayud A, Ferroni L, Goltsev V, Guidi L,**  
1133 **Jajoo A, Li P, Losciale P, Mishra VK, Misra AN, Nebauer SG, Pancaldi S, Penella C,**  
1134 **Pollastrini M, Suresh K, Tambussi E, Yanniccari M, Zivcak M, Cetner MD,**  
1135 **Samborska IA, Stírbet A, Olsovska K, Kunderlikova K, Shelonzek H, Rusinowski S,**  
1136 **Baba W** (2017) Frequently asked questions about chlorophyll fluorescence, the sequel.

- 1137           Photosynth Res **132**: 13-66
- 1138 **Kirst H, Formighieri C, Melis A** (2014) Maximizing photosynthetic efficiency and culture  
1139 productivity in cyanobacteria upon minimizing the phycobilisome light-harvesting antenna  
1140 size. *Bba-Bioenergetics* **1837**: 1653-1664
- 1141 **Kirst H, Gabilly ST, Niyogi KK, Lemaux PG, Melis A** (2017) Photosynthetic antenna  
1142 engineering to improve crop yields. *Planta* **245**: 1009-1020
- 1143 **Kirst H, Garcia-Cerdan JG, Zurbriggen A, Melis A** (2012) Assembly of the light-harvesting  
1144 chlorophyll antenna in the green alga *Chlamydomonas reinhardtii* requires expression of the  
1145 TLA2-CpFTSY gene. *Plant Physiol* **158**: 930-945
- 1146 **Kirst H, Garcia-Cerdan JG, Zurbriggen A, Ruehle T, Melis A** (2012) Truncated photosystem  
1147 chlorophyll antenna size in the green microalga *Chlamydomonas reinhardtii* upon deletion  
1148 of the TLA3-CpSRP43 gene. *Plant Physiol* **160**: 2251-2260
- 1149 **Kirst H, Melis A** (2014) The chloroplast signal recognition particle (CpSRP) pathway as a tool to  
1150 minimize chlorophyll antenna size and maximize photosynthetic productivity. *Biotechnol*  
1151 *Adv* **32**: 66-72
- 1152 **Kirst H, Shen Y, Vamvaka E, Betterle N, Xu D, Warek U, Strickland JA, Melis A** (2018)  
1153 Downregulation of the CpSRP43 gene expression confers a truncated light-harvesting  
1154 antenna (TLA) and enhances biomass and leaf-to-stem ratio in *Nicotiana tabacum* canopies.  
1155 *Planta* **248**: 139-154
- 1156 **Kugelmann M, Fausser A, Ossenbuhl F, Brennicke A** (2013) Phenotypes of Alb3p and  
1157 carotenoid synthesis mutants show similarities regarding light sensitivity, thylakoid structure  
1158 and protein stability. *Photosynthetica* **51**: 45-54
- 1159 **Kumar S, Stecher G, Tamura K** (2016) MEGA7: Molecular Evolutionary Genetics Analysis  
1160 Version 7.0 for Bigger Datasets. *Mol Biol Evol* **33**: 1870-1874
- 1161 **Lamb J, Forfang K, Hohmann-Marriott M** (2015) A practical solution for 77 K fluorescence  
1162 measurements based on LED excitation and CCD array detector. *PLoS One* **10**: e0132258
- 1163 **Lang M, Kroth PG** (2001) Diatom fucoxanthin chlorophyll a/c-binding protein (FCP) and land  
1164 plant light-harvesting proteins use a similar pathway for thylakoid membrane Insertion. *J*  
1165 *Biol Chem* **276**: 7985-7991
- 1166 **Lavaud J, Goss R** (2014) The peculiar features of non-photochemical fluorescence quenching in  
1167 diatoms and brown algae. *In* B Demmig-Adams, G Garab, IW Adams, Govindjee, eds, Non-  
1168 photochemical quenching and energy dissipation in plants, algae and cyanobacteria.  
1169 *Advances in photosynthesis and respiration (Including bioenergy and related processes)*, Vol  
1170 40. Springer, Dordrecht
- 1171 **Lavaud J, Lepetit B** (2013) An explanation for the inter-species variability of the photoprotective  
1172 non-photochemical chlorophyll fluorescence quenching in diatoms. *Biochim Biophys Acta*  
1173 **1827**: 294-302
- 1174 **Lavaud J, Rousseau B, van Gorkom HJ, Etienne AL** (2002) Influence of the diadinoxanthin pool  
1175 size on photoprotection in the marine planktonic diatom *Phaeodactylum tricorutum*. *Plant*  
1176 *Physiol* **129**: 1398-1406
- 1177 **Le SQ, Gascuel O** (2008) An improved general amino acid replacement matrix. *Mol Biol Evol* **25**:  
1178 1307-1320
- 1179 **Lepetit B, Gelin G, Lepetit M, Sturm S, Vugrinec S, Rogato A, Kroth PG, Falciatore A,**  
1180 **Lavaud J** (2017) The diatom *Phaeodactylum tricorutum* adjusts nonphotochemical  
1181 fluorescence quenching capacity in response to dynamic light via fine-tuned Lhcx and  
1182 xanthophyll cycle pigment synthesis. *New Phytol* **214**: 205-218
- 1183 **Lepetit B, Goss R, Jakob T, Wilhelm C** (2012) Molecular dynamics of the diatom thylakoid

1184 membrane under different light conditions. *Photosynth Res* **111**: 245-257

1185 **Lepetit B, Sturm S, Rogato A, Gruber A, Sachse M, Falciatore A, Kroth PG, Lavaud J** (2013)

1186 High light acclimation in the secondary plastids containing diatom *Phaeodactylum*

1187 *tricornutum* is triggered by the redox state of the plastoquinone pool. *Plant Physiol* **161**:

1188 853-865

1189 **Lepetit B, Volke D, Gilbert M, Wilhelm C, Goss R** (2010) Evidence for the existence of one

1190 antenna-associated, lipid-dissolved and two protein-bound pools of diadinoxanthin cycle

1191 pigments in diatoms. *Plant Physiol* **154**: 1905-1920

1192 **Lewis NE, Marty NJ, Kathir KM, Rajalingam D, Kight AD, Daily A, Kumar TK, Henry RL,**

1193 **Goforth RL** (2010) A dynamic cpSRP43-Albino3 interaction mediates translocase

1194 regulation of chloroplast signal recognition particle (cpSRP)-targeting components. *J Biol*

1195 *Chem* **285**: 34220-34230

1196 **Madhuri S, Serif M, Rio Bartulos C, Lepetit B, Kroth PG** (2019) A strategy to complement

1197 PtAUREO1a in TALEN knockout strains of *Phaeodactylum tricornutum*. *Algal Res* **39**:

1198 101469

1199 **Melis A** (1989) Spectroscopic methods in photosynthesis - Photosystem stoichiometry and

1200 chlorophyll antenna size. *Philos T Roy Soc B* **323**: 397-409

1201 **Melis A, Brown JS** (1980) Stoichiometry of system I and system II reaction centers and of

1202 plastoquinone in different photosynthetic membranes. *P Natl Acad Sci-Biol* **77**: 4712-4716

1203 **Miloslavina Y, Grouneva I, Lambrev PH, Lepetit B, Goss R, Wilhelm C, Holzwarth AR**

1204 (2009) Ultrafast fluorescence study on the location and mechanism of non-photochemical

1205 quenching in diatoms. *Biochim Biophys Acta* **1787**: 1189-1197

1206 **Mock T, Otilar RP, Strauss J, McMullan M, Paajanen P, Schmutz J, Salamov A, Sanges R,**

1207 **Toseland A, Ward BJ, Allen AE, Dupont CL, Frickenhaus S, Maumus F, Veluchamy**

1208 **A, Wu T, Barry KW, Falciatore A, Ferrante MI, Fortunato AE, Glöckner G, Gruber**

1209 **A, Hipkin R, Janech MG, Kroth PG, Leese F, Lindquist EA, Lyon BR, Martin J,**

1210 **Mayer C, Parker M, Quesneville H, Raymond JA, Uhlig C, Valas RE, Valentin KU,**

1211 **Worden AZ, Armbrust EV, Clark MD, Bowler C, Green BR, Moulton V, van**

1212 **Oosterhout C, Grigoriev IV** (2017) Evolutionary genomics of the cold-adapted diatom

1213 *Fragilariopsis cylindrus*. *Nature* **541**: 536

1214 **Moore M, Harrison MS, Peterson EC, Henry R** (2000) Chloroplast Oxa1p homolog albino3 is

1215 required for post-translational integration of the light harvesting chlorophyll-binding protein

1216 into thylakoid membranes. *J Biol Chem* **275**: 1529-1532

1217 **Nelson N, Yocum CF** (2006) Structure and function of photosystems I and II. *Annu Rev Plant Biol*

1218 **57**: 521-565

1219 **Nicholas KB, Nicholas HBJ, Deerfield DWI** (1997) GeneDoc: analysis and visualization of

1220 genetic variation. . *EMBNEW.NEWS* **4**

1221 **Nymark M, Sharma AK, Hafskjold MC, Sparstad T, Bones AM, Winge P** (2017)

1222 CRISPR/Cas9 Gene editing in the marine diatom *Phaeodactylum tricornutum*. *Bio-protocol*

1223 **7**: e2442

1224 **Nymark M, Sharma AK, Sparstad T, Bones AM, Winge P** (2016) A CRISPR/Cas9 system

1225 adapted for gene editing in marine algae. *Sci Rep-Uk* **6**

1226 **Nymark M, Valle KC, Brembu T, Hancke K, Winge P, Andresen K, Johnsen G, Bones AM**

1227 (2009) An integrated analysis of molecular acclimation to high light in the marine diatom

1228 *Phaeodactylum tricornutum*. *PLoS ONE* **4**: e7743

1229 **Nymark M, Valle KC, Hancke K, Winge P, Andresen K, Johnsen G, Bones AM, Brembu T**

1230 (2013) Molecular and photosynthetic responses to prolonged darkness and subsequent



1231 acclimation to re-illumination in the diatom *Phaeodactylum tricornutum*. PLoS ONE **8**:  
1232 e58722

1233 **Oey M, Ross IL, Stephens E, Steinbeck J, Wolf J, Radzun KA, Kugler J, Ringsmuth AK,**  
1234 **Kruse O, Hankamer B** (2013) RNAi knock-down of LHCBM1, 2 and 3 Increases  
1235 photosynthetic H<sub>2</sub> production efficiency of the green alga *Chlamydomonas reinhardtii*. Plos  
1236 One **8**

1237 **Ossenbühl F, Gohre V, Meurer J, Krieger-Liszak A, Rochaix JD, Eichacker LA** (2004)  
1238 Efficient assembly of photosystem II in *Chlamydomonas reinhardtii* requires Alb3.1p, a  
1239 homolog of *Arabidopsis* ALBINO3. Plant Cell **16**: 1790-1800

1240 **Oudot-Le Secq MP, Grimwood J, Shapiro H, Armbrust EV, Bowler C, Green BR** (2007)  
1241 Chloroplast genomes of the diatoms *Phaeodactylum tricornutum* and *Thalassiosira*  
1242 *pseudonana*: comparison with other plastid genomes of the red lineage. Mol Genet  
1243 Genomics **277**: 427-439

1244 **Polle JE, Kanakagiri SD, Melis A** (2003) Tla1, a DNA insertional transformant of the green alga  
1245 *Chlamydomonas reinhardtii* with a truncated light-harvesting chlorophyll antenna size.  
1246 Planta **217**: 49-59

1247 **Powles SB, Critchley C** (1980) Effect of light intensity during growth on photoinhibition of intact  
1248 attached bean leaflets. Plant Physiol **65**: 1181-1187

1249 **Premvardhan L, Bordes L, Beer A, Büchel C, Robert B** (2009) Carotenoid structures and  
1250 environments in trimeric and oligomeric fucoxanthin chlorophyll *a/c*<sub>2</sub> proteins from  
1251 resonance Raman spectroscopy. J Phys Chem B **113**: 12565-12574

1252 **Premvardhan L, Robert B, Beer A, Büchel C** (2010) Pigment organization in fucoxanthin  
1253 chlorophyll *a/c*<sub>2</sub> proteins (FCP) based on resonance Raman spectroscopy and sequence  
1254 analysis. Biochim Biophys Acta **1797**: 1647-1656

1255 **Ramakers C, Ruijter JM, Deprez RH, Moorman AF** (2003) Assumption-free analysis of  
1256 quantitative real-time polymerase chain reaction (PCR) data. Neurosci Lett **339**: 62-66

1257 **Rodriguez F, Chauton M, Johnsen G, Andresen K, Olsen LM, Zapata M** (2006)  
1258 Photoacclimation in phytoplankton: implications for biomass estimates, pigment  
1259 functionality and chemotaxonomy. Mar Biol **148**: 963-971

1260 **Ruijter JM, Ramakers C, Hoogaars WM, Karlen Y, Bakker O, van den Hoff MJ, Moorman**  
1261 **AF** (2009) Amplification efficiency: linking baseline and bias in the analysis of quantitative  
1262 PCR data. Nucleic Acids Res **37**: e45

1263 **Saitou N, Nei M** (1987) The neighbor-joining method: a new method for reconstructing  
1264 phylogenetic trees. Mol Biol Evol **4**: 406-425

1265 **Sakshaug E, Bricaud A, Dandonneau Y, Falkowski PG, Kiefer DA, Legendre L, Morel A,**  
1266 **Parslow J, Takahashi M** (1997) Parameters of photosynthesis: definitions, theory and  
1267 interpretation of results. J Plankton Res **19**: 1637-1670

1268 **Schuenemann D, Gupta S, Persello-Cartieaux F, Klimyuk VI, Jones JD, Nussaume L,**  
1269 **Hoffman NE** (1998) A novel signal recognition particle targets light-harvesting proteins to  
1270 the thylakoid membranes. Proc Natl Acad Sci U S A **95**: 10312-10316

1271 **Serif M, Lepetit B, Weißert K, Kroth PG, Rio Bartulos C** (2017) A fast and reliable strategy to  
1272 generate TALEN-mediated gene knockouts in the diatom *Phaeodactylum tricornutum*. Algal  
1273 Res **23**: 186-195

1274 **Serôdio J, Vieira S, Cruz S, Coelho H** (2006) Rapid light-response curves of chlorophyll  
1275 fluorescence in microalgae: relationship to steady-state light curves and non-photochemical  
1276 quenching in benthic diatom-dominated assemblages. Photosynth Res **90**: 29-43

1277 **Sundberg E, Slagter JG, Fridborg I, Cleary SP, Robinson C, Coupland G** (1997) ALBINO3,

1278 an Arabidopsis nuclear gene essential for chloroplast differentiation, encodes a chloroplast  
1279 protein that shows homology to proteins present in bacterial membranes and yeast  
1280 mitochondria. *Plant Cell* **9**: 717-730

1281 **Taddei L, Chukhutsina VU, Lepetit B, Stella GR, Bassi R, van Amerongen H, Bouly JP,**  
1282 **Jaubert M, Finazzi G, Falcatore A** (2018) Dynamic changes between two LHCX-related  
1283 energy quenching sites control diatom photoacclimation. *Plant Physiol* **177**: 953-965

1284 **Taddei L, Stella GR, Rogato A, Bailleul B, Fortunato AE, Annunziata R, Sanges R, Thaler M,**  
1285 **Lepetit B, Lavaud J, Jaubert M, Finazzi G, Bouly JP, Falcatore A** (2016) Multisignal  
1286 control of expression of the LHCX protein family in the marine diatom *Phaeodactylum*  
1287 *tricornutum*. *J Exp Bot* **67**: 3939-3951

1288 **Theis J, Schroda M** (2016) Revisiting the photosystem II repair cycle. *Plant Signal Behav* **11**:  
1289 e1218587

1290 **Thompson JD, Gibson TJ, Plewniak F, Jeanmougin F, Higgins DG** (1997) The CLUSTAL\_X  
1291 windows interface: flexible strategies for multiple sequence alignment aided by quality  
1292 analysis tools. *Nucleic Acids Res* **25**: 4876-4882

1293 **Träger C, Rosenblad MA, Ziehe D, Garcia-Petit C, Schrader L, Kock K, Richter CV,**  
1294 **Klinkert B, Narberhaus F, Herrmann C, Hofmann E, Aronsson H, Schunemann D**  
1295 (2012) Evolution from the prokaryotic to the higher plant chloroplast signal recognition  
1296 particle: the signal recognition particle RNA is conserved in plastids of a wide range of  
1297 photosynthetic organisms. *Plant Cell* **24**: 4819-4836

1298 **Valle KC, Nymark M, Aamot I, Hancke K, Winge P, Andresen K, Johnsen G, Brembu T,**  
1299 **Bones AM** (2014) System responses to equal doses of photosynthetically usable radiation of  
1300 blue, green, and red light in the marine diatom *Phaeodactylum tricornutum*. *PLoS One* **9**:  
1301 e114211

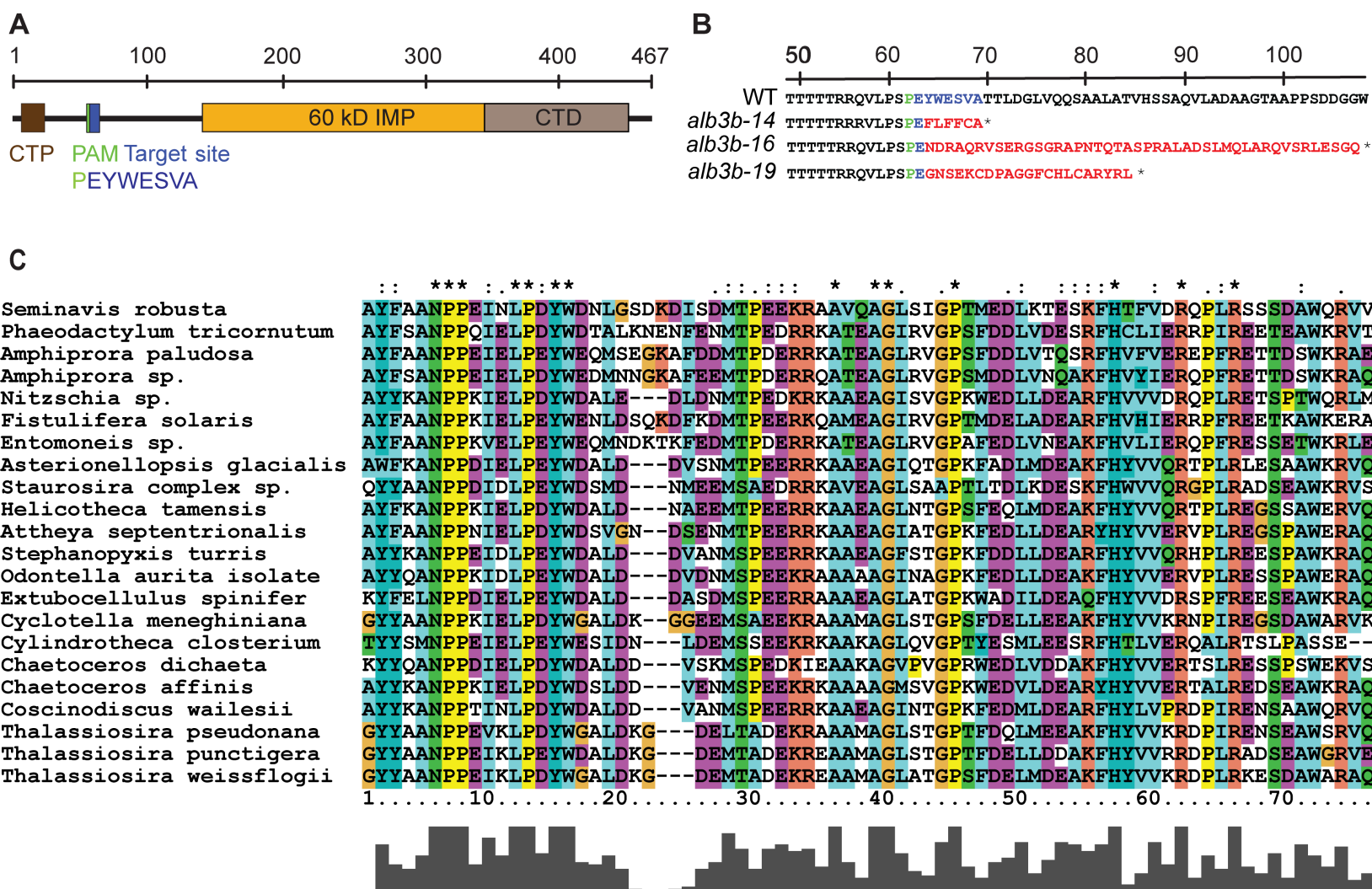
1302 **Yamagishi A, Ikeda Y, Komura M, Koike H, Satoh K, Itoh S, Shibata Y** (2010) Shallow sink in  
1303 an antenna pigment system of photosystem I of a marine centric diatom, *Chaetoceros*  
1304 *gracilis*, revealed by ultrafast fluorescence spectroscopy at 17 K. *J Phys Chem B* **114**: 9031-  
1305 9038

1306 **Wang W, Yu L-J, Xu C, Tomizaki T, Zhao S, Umena Y, Chen X, Qin X, Xin Y, Suga M, Han**  
1307 **G, Kuang T, Shen J-R** (2019) Structural basis for blue-green light harvesting and energy  
1308 dissipation in diatoms. *Science* **363**: eaav0365

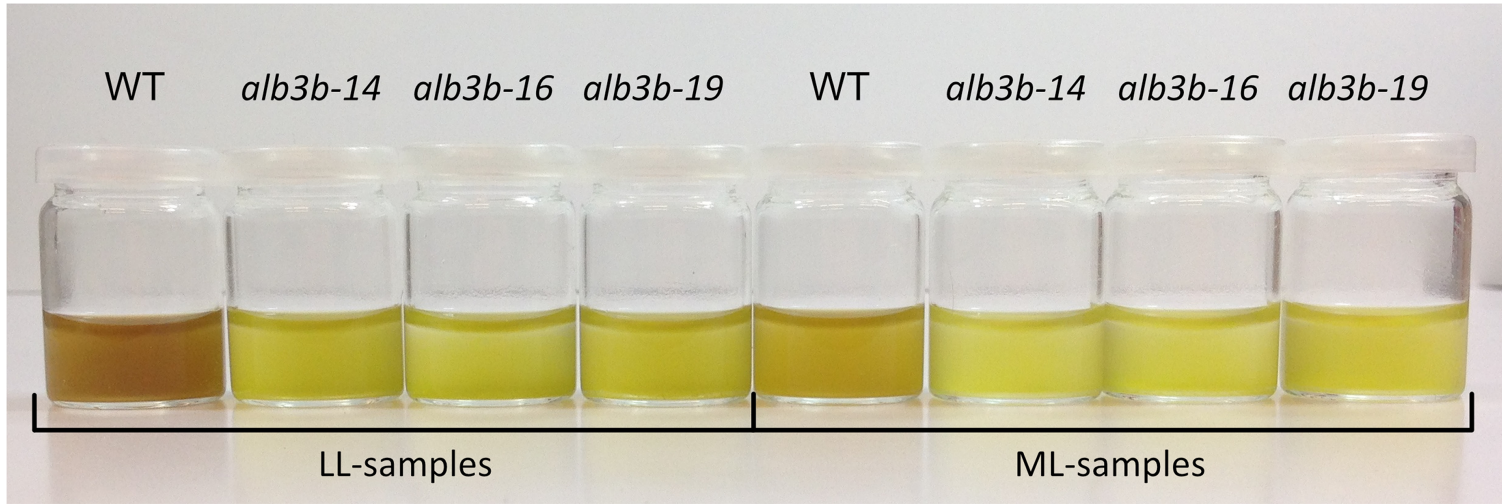
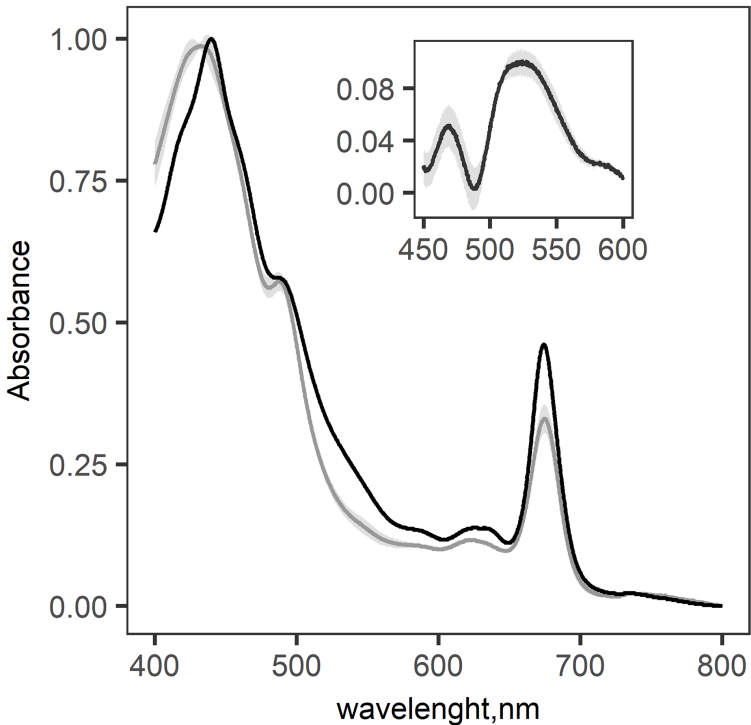
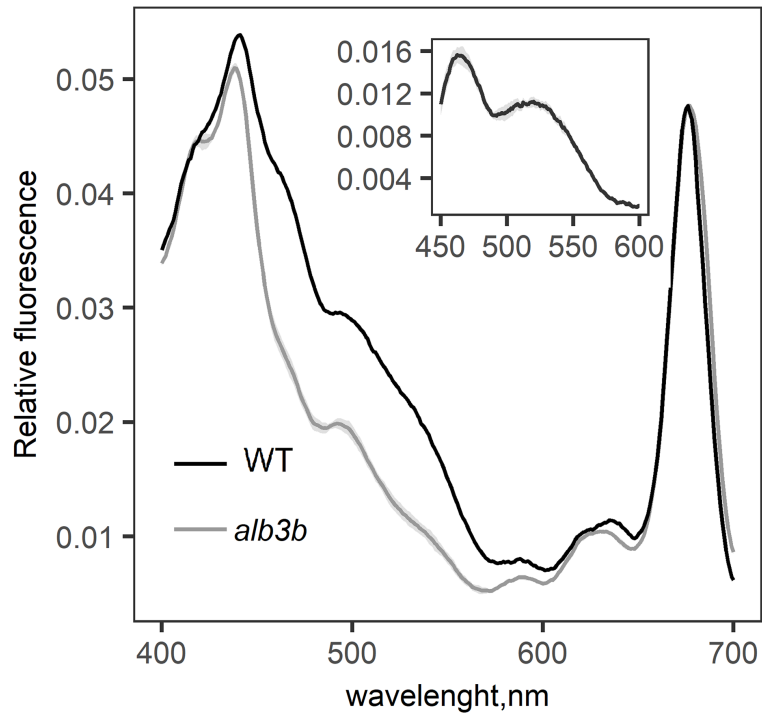
1309

1310

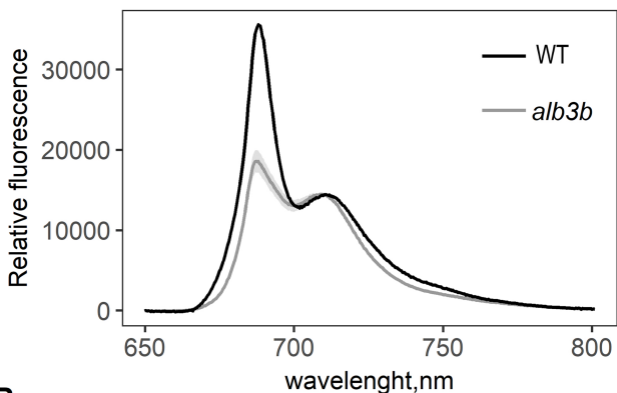
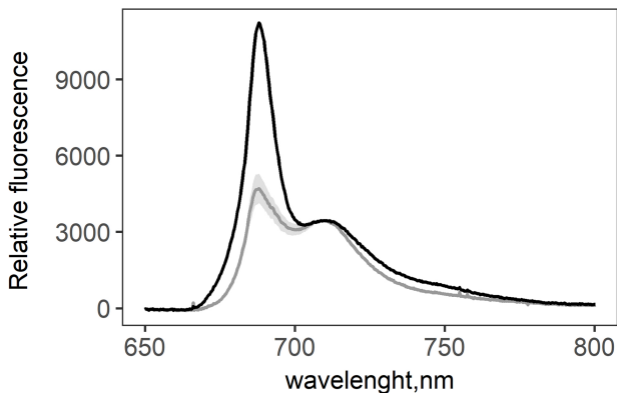
1311



**Figure 1: Presentation of intact and truncated ALB3b protein.** A) The area of the ALB3b protein corresponding to the 20 bp target region for CRISPR/Cas9-based gene editing is located toward the N-terminal part of the protein (blue highlighting) with the PAM site located at the reverse DNA strand (green highlighting). CTP: Chloroplast targeting peptide; 60 kD IMP: 60 kD Inner Membrane Protein domain; CTD: conserved C-terminal domain. B) Overview of amino acid sequences resulting from CRISPR/Cas9 induced inserts in the three *alb3b* KO lines causing premature stop codons and truncated ALB3b proteins. Color coding: Blue: WT target sequence; Green: amino acid corresponding to PAM site; Red letters: Insert; \*: Premature stop. C) Protein alignment based on the C-terminal domain (CTD) of ALB3b proteins in diatoms.

**A****B****C**

**Figure 2. Color differences and spectral characteristics of WT and *alb3b* mutants.** A) Visual representation of the *alb3b* phenotype compared to WT at low light (LL; 35  $\mu\text{mol photons m}^{-2} \text{s}^{-1}$ ; left side) and ML (200  $\mu\text{mol photons m}^{-2} \text{s}^{-1}$ ; right side). For comparison and visualization of the color differences, all cultures were adjusted to equal cell densities ( $3 \times 10^7$  cells/ml) B) Absorbance spectra and C) in vivo fluorescence excitation spectra of cultures acclimated to ML. Isolated intact thylakoid membranes were used for recording of the absorption spectra to avoid scattering. Fluorescence emission was measured at 730 nm to ensure origin from the reaction center II Chl *a*. Insets: Difference spectra between: the absorbance of WT and *alb3b* KO lines B), and excitation energy transfer in the blue-green region of the in vivo fluorescence excitation spectra C). WT: Presented as an average of three biological replicates; *alb3b*: Presented as an average of the three *alb3b* KO lines 14, 16 and 19 with  $\pm$ SD for all data points indicated by the grey area around the graphs. Three biological replicates were measured for each line.

**A****B**

**Figure 3. 77 K fluorescence emission spectra of WT and *alb3b* KO samples acclimated to ML.** Samples were excited at either 435 nm (A) or 470 nm (B). The emission spectra were normalized at their 710 nm maximum. Data for *alb3b* is an average of the three *alb3b* KO lines 14, 16 and 19 with  $\pm$ SD for all data points indicated by the grey area around the graphs. Three biological replicates were measured for each line including the WT.

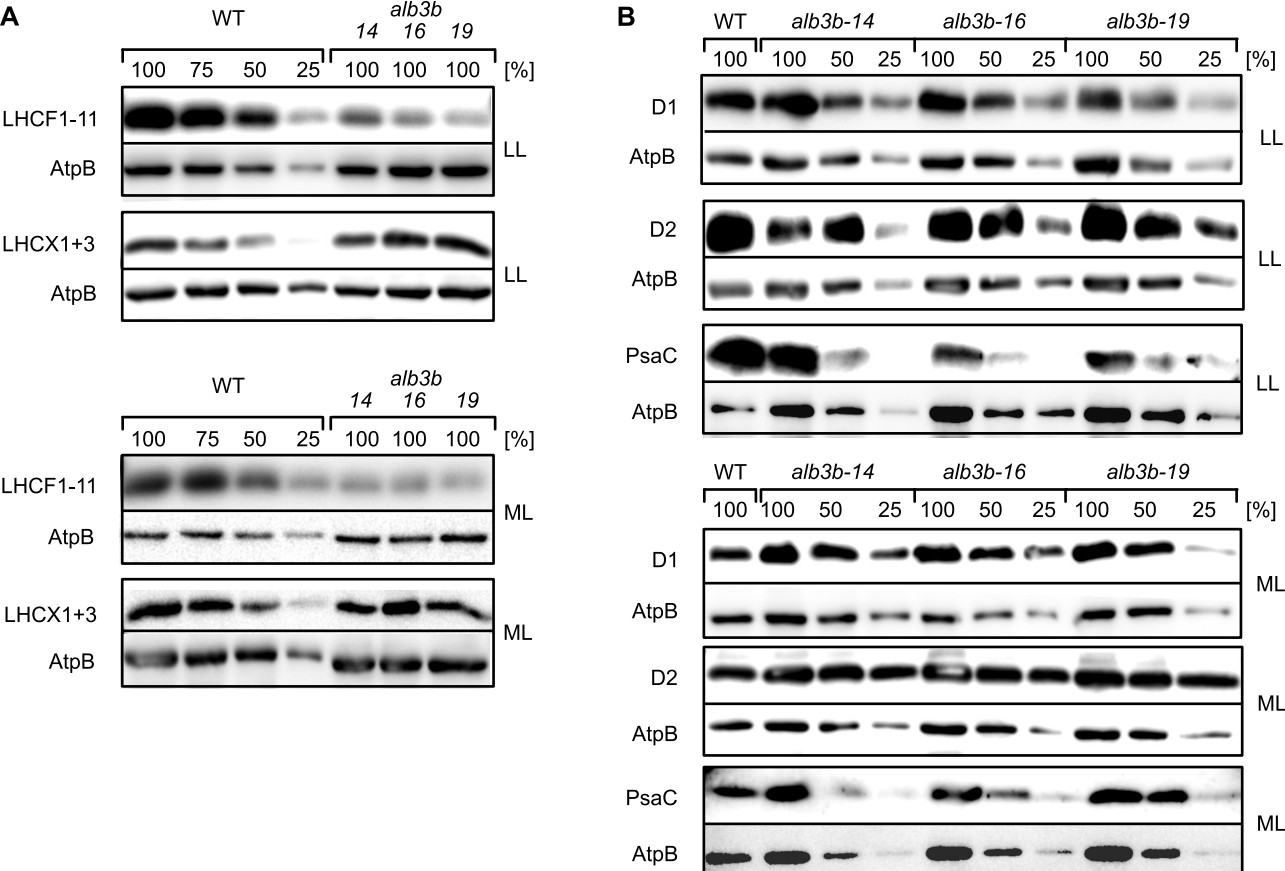


**Figure 4. Western blot analysis of thylakoid membrane proteins from WT and *alb3b* mutant lines acclimated to low light (LL; 35  $\mu\text{mol photons m}^{-2} \text{s}^{-1}$ ) or medium light (ML; 200  $\mu\text{mol photons m}^{-2} \text{s}^{-1}$ ) conditions.** A) Abundance of LHC proteins belonging to the LHCf group were evaluated using an antibody recognizing LHCf1-11, whereas the LHCX proteins were recognized by anti-FCP6 (a LHCX family member of *C. meneghiniana*). A dilution series of the WT samples were used to assess the level of LHC proteins in *alb3b* mutants compared to WT. B) Protein expression of PSII and PSI core proteins were evaluated with antibodies against the D1 (PSII), D2 (PSII) and PsaC (PSI) core subunits. A dilution series of the *alb3b* samples were used to assess the level of photosystem subunits in *alb3b* mutants compared to WT. An antibody recognizing the  $\beta$ -subunit of ATP synthase (AtpB) were used as loading control on each of the individual blots. Lanes marked with 100% contain 10  $\mu\text{g}$  (20  $\mu\text{g}$  for analysis of LHCX levels) of protein extracts. Images have been cropped.

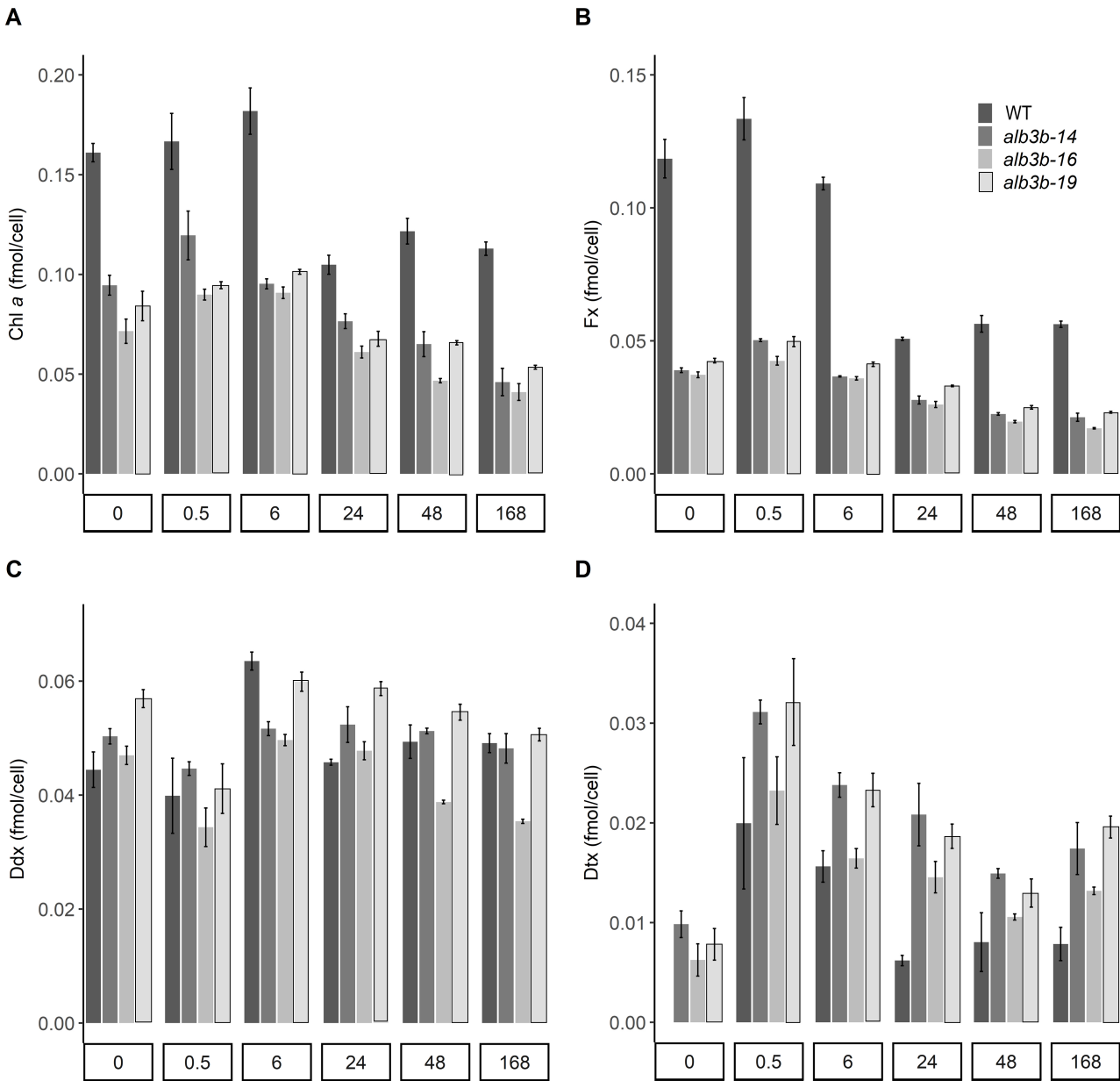


**Figure 5. Pigment concentrations per cell for WT and *alb3b* mutant lines as a function of ML exposure time.** Cellular pigment concentrations of A) Chl a, B) Fx, C) Ddx and D) Dtx in WT and *alb3b* mutant cells as a function of time following a shift from LL conditions (0 h; 35  $\mu\text{mol photons m}^{-2} \text{s}^{-1}$ ) to ML conditions (200  $\mu\text{mol photons m}^{-2} \text{s}^{-1}$ ) for 0.5, 6, 24, 48 and 168 h. Results are presented as a mean of three biological replicates with  $\pm$ SD.

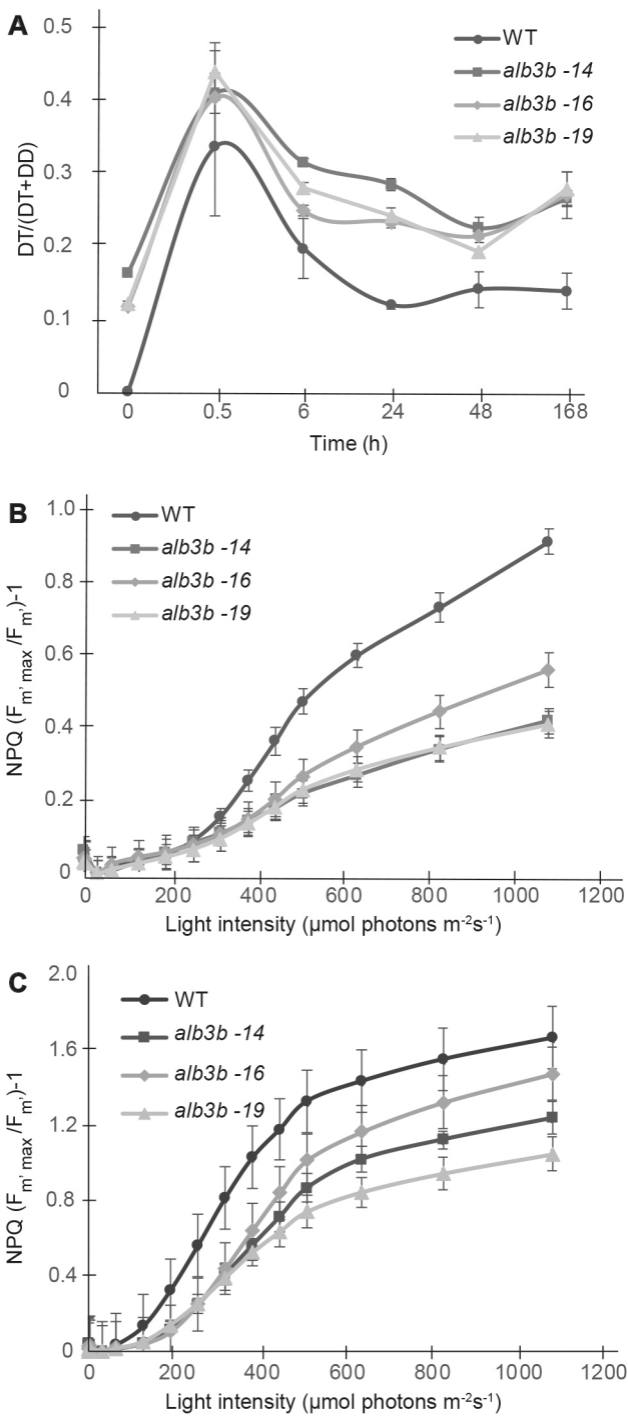


**Figure 6. De-epoxidation state index and NPQ capacity of WT and *alb3b* mutants.** A) De-epoxidation state index (DES =  $D_{tx}/(D_{tx} + D_{dx})$ ) calculated from the HPLC pigment data from LL acclimated (0 h) WT and *alb3b* cultures exposed to ML for 0.5, 6, 24, 48 and 168 h. B) Capacity for NPQ calculated from rapid light curves derived from LL acclimated cells approx. two months after isolation of mutated single cells and C) after being maintained in culture for one more year.  $NPQ = (F_{m'_{max}}/F_{m'}) - 1$ .  $F_{m'_{max}}$  replaces the commonly used  $F_m$  since  $F_m$  values frequently occur that are higher than the  $F_m$  from dark-treated diatom samples (Serodio et al., 2006). Results are presented as a mean of three biological replicates with  $\pm$ SD.



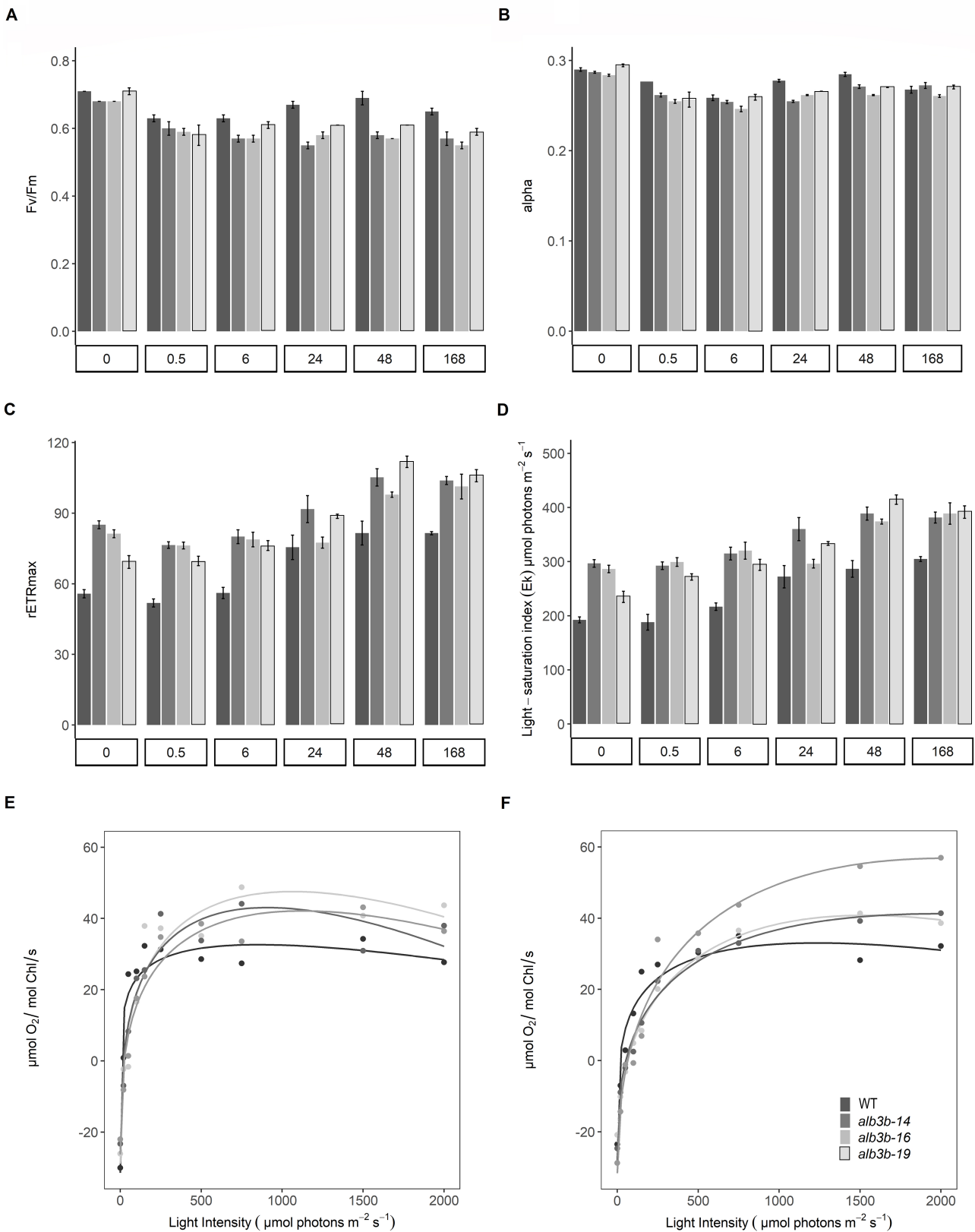


**Figure 7. Photo-physiological responses of WT and *alb3b* mutant lines.** In vivo Chl *a* fluorescence kinetics (PAM) were used to estimate A) the maximum quantum yield of PSII (Fv/Fm), B) the maximum light utilization coefficient ( $\alpha$ ), C) the maximum relative light-saturated electron transport rate (rETRmax) and D) the light saturation index (Ek) in LL (0h) acclimated WT and *alb3b* KO lines as a function of ML exposure time (0.5-168 h). Values are presented with  $\pm$ SD bars. Light-saturation curves of photosynthesis based on oxygen evolution were produced for E) LL acclimated and F) ML acclimated WT and *alb3b* KO lines. The oxygen concentration was normalized on a per-Chl basis. The results were fit with curves based on a polynomial regression using R. All values are presented as an average of three biological replicates.



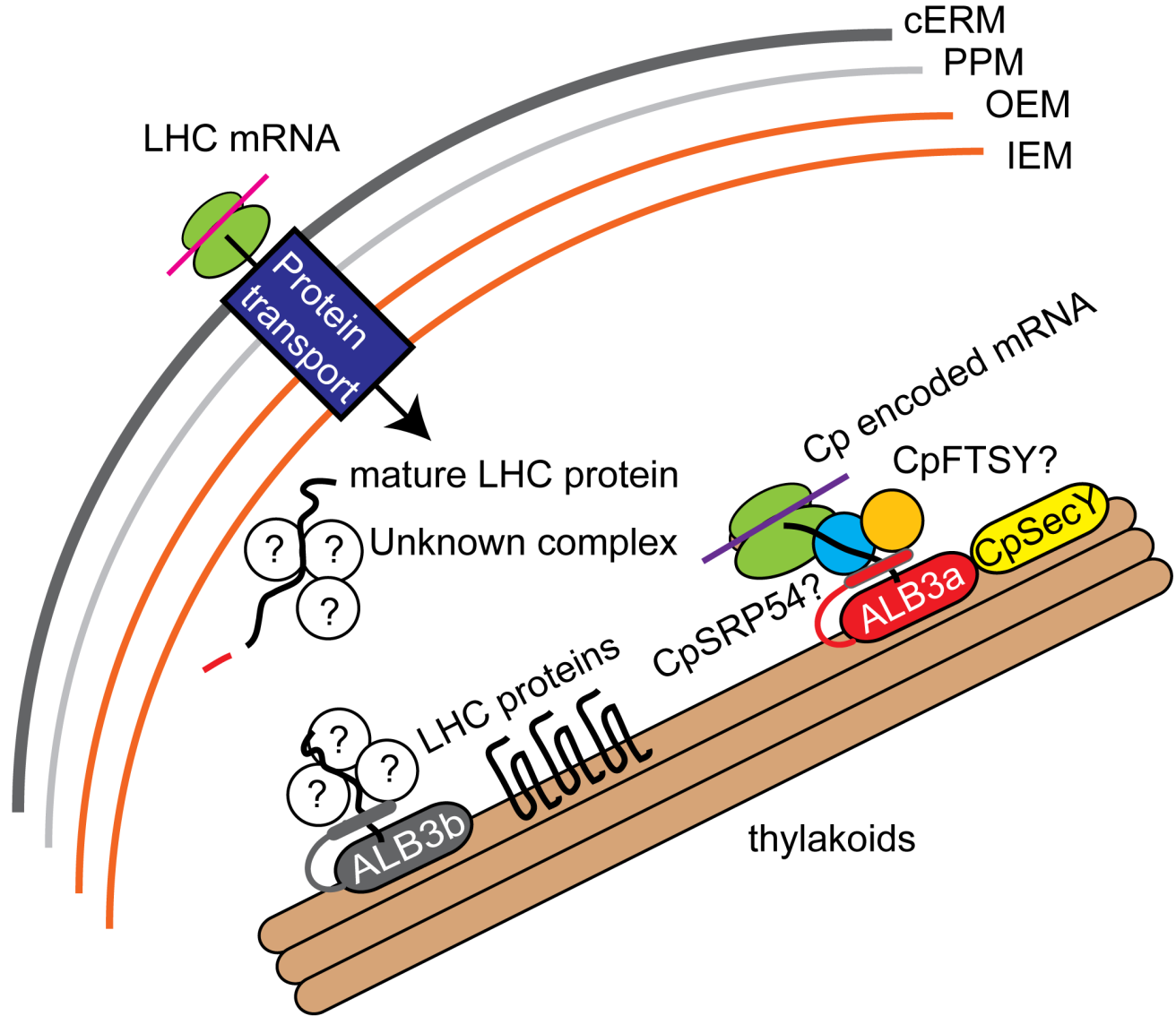


**Figure 9. Proposed model of the role of diatom ALB3 insertases in insertion/assembly of thylakoid membrane proteins.** LHC proteins are synthesized on ribosomes on the cERM, transported through the four membranes surrounding the secondary plastid of diatoms, and guided to ALB3b by an unknown protein complex before incorporation into the thylakoid membrane (left side). Chloroplast-encoded proteins are suggested to be integrated by the co-translational cpSRP pathway including cpSRP54, FTSY and ALB3ba (right side). cERM: chloroplast ER membrane; PPM: periplastidal membrane; OEM: plastid outer envelope membrane; IEM: plastid inner envelope membrane. CpSRP54: chloroplast signal recognition particle protein 54; CpFTSY: chloroplast SRP receptor; ALB3: chloroplast SRP insertase Albino3.